Nanoscale Advances

ROYAL SOCIETY OF CHEMISTRY

REVIEW

View Article Online
View Journal | View Issue

Cite this: *Nanoscale Adv.*, 2021, **3**, 6271

Advances in wearable textile-based micro energy storage devices: structuring, application and perspective

Yixue Duan,[ab] Gongchuan You,[a] Kaien Sun,[a] Zhe Zhu,[ab] Xiaoqiao Liao,[a] Linfeng Lv,[ab] Hui Tang,[d] Bin Xu*[ae] and Liang He*[abc]

Received 30th June 2021
Accepted 11th September 2021

DOI: 10.1039/d1na00511a

rsc.li/nanoscale-advances

The continuous expansion of smart microelectronics has put forward higher requirements for energy conversion, mechanical performance, and biocompatibility of micro-energy storage devices (MESDs). Unique porosity, superior flexibility and comfortable breathability make the textile-based structure a great potential in wearable MESDs. Herein, a timely and comprehensive review of this field is provided according to recent research advances. The following aspects, device construction of textile-based MESDs (TMESDs), fabric processing of textile components and smart functionalization (*e.g.*, mechanical reliability, energy harvesting, sensing, self-charging and self-healing, *etc.*) are discussed and summarized thoroughly. Also, the perspectives on the microfabrication processes and multiple applications of TMESDs are elaborated.

1. Introduction

The field of portable electronics is gradually broadening as an essential concomitant for decades with the development of the Internet of Things (IoT).[1–4] Among them, the combination of artificial intelligence and highly integrated microelectronics has derived significant advantages and many applications are developed, such as electronic textiles,[5] intelligent sensor[6] and smart medical implant.[7] Miniaturized components and microfabrication processes endow micro energy storage devices (MESDs) with high energy density for practical applications. Based on requirements of energy supply, the fabricated MESDs should show desirable flexibility and durability for practical applications. However, most of the MESDs under chemical and mechanical strain will form multiple fractures and eventually lose electrical contact. Therefore, apart from favorable electrochemical performance, it is also a challenge for such a micropower source to have excellent mechanical performance.[8]

Textiles serve as the daily necessities with a rich history dating back thousands of years and are attracting much attention because of their unique porosity and high flexibility.[9–11] The rough and porous structure of textiles is beneficial for high electron transport, and can be bent, twisted even rolled up without any cracks caused by the bending stress, resulting in both outstanding electrical and mechanical performance (Scheme 1).[12]

Generally, the contribution of textiles to the micro device/system is mainly reflected in the following aspects. For fibers with large microscopic diameters, nanostructures can be built inside or on the surface to achieve the goal of overall modification. Spinning technology that adds conductive functional materials to the precursor is developed rapidly in recent years.[13] Electrospinning technology acting under high electric potential produces fibers with a diameter at a nanometer scale, such as carbon nanofibers with high electrical conductivity and large-range stretchability.[20] Simultaneously, the all-fiber structured textile-based pressure sensor made by this strategy has the desired sensing accuracy.[21] Modifying the surface of textile is also a feasible processing method. Among them, printing technology can selectively deposit electronic components, and the compatibility of printing ink for textile allows the microelectrode composed of conductive layers to directly cover the surface of the textile. Furthermore, a single fiber embedded with electronic function can be woven into large-area clothing fabric. Crisscross networked structure endows fabric ductility, achieving a large-scale extension of electronic functions, such as electroluminescence. Processing fabrics at different dimensions satisfies the customized construction of devices.

In terms of energy conversion equipment, MESDs such as microbattery (MB) and microsupercapacitor (MSC) possess significant advantages. In the matter of appearance, high integration of MESDs provides the device with multifunction and

[a]*School of Mechanical Engineering, Sichuan University, Chengdu 610065, P. R. China. E-mail: hel20@scu.edu.cn; bin_xu@outlook.com*
[b]*State Key Laboratory of Advanced Technology for Materials Synthesis and Processing, Wuhan University of Technology, Wuhan 430070, P. R. China*
[c]*Med+X Center for Manufacturing, West China Hospital, Sichuan University, Chengdu 610041, P. R. China*
[d]*School of Materials and Energy, University of Electronic Science and Technology of China, Chengdu 611731, P. R. China*
[e]*Science and Technology on Reactor Fuel and Materials Laboratory, Chengdu 610095, P. R. China*

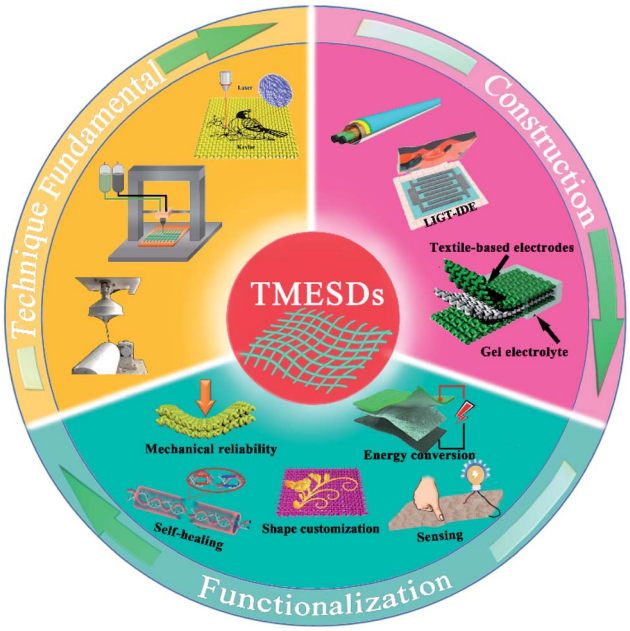

Scheme 1 A concept map of TMESDs. "Construction": reproduced with permission.[13] Copyright 2016, American Association for the Advancement of Science. Reproduced with permission.[14] Copyright 2019, American Chemical Society. Reproduced with permission.[15] Copyright 2021, Elsevier. "Technique fundamental": reproduced with permission.[16] Copyright 2021, Elsevier. Reproduced with permission.[17] Copyright 2020, De Gruyter. Reproduced with permission.[18] Copyright 2020, American Chemical Society. "Functionalization": reproduced with permission.[19] Copyright 2019, American Chemical Society.

compact construction that is tailored to portability. For energy loading, miniaturized electrochemical equipment ensures high energy density and stable voltage output. MSCs have an ultra-high power density, long operating lifetime[22] (>100 000 cycles) and fast charge/discharge in seconds.[23] While MBs have more advantages in energy storage owing to their outstanding energy density. To date, wearable devices have increasing requirements on textile-based MESDs (TMESDs), such as electronic skin (e-skin),[24] and textile-based displays.[25] According to the type of microelectrode, MESDs can be divided into sandwiched thin-film MESDs,[26] interdigital MESDs[27] and fiber-type MESDs.[28] Specifically, fiber-shaped miniaturized devices possess unique one-dimensional (1D) ductility and intrinsic knittability due to high-aspect-ratio fibers. The main challenges for fiber-shaped microdevices are ascribed to the preparation of functional nanomaterials for hybrid fiber electrodes and the integration with other components. Compared with the 1D structure, it is more convenient to obtain stacked micro/nano structures and interlayer functionalization in the 2D planer structure.[28,29] Interdigital devices fabricated by constructing process with elaborate parallel finger-shaped microelectrodes facilitate higher energy loading and adjustable width for fast ion transport in the microelectrode. Simultaneously, it puts forward extremely strict requirements on the micromachining process. The uneven surface of the fabric, for example, facilitates the production of lithographic patterns. In addition to micromachining accuracy, the compatibility between material and the textile substrate should be taken into account as well. As an instance, laser engraving utilizing the thermal energy of laser beam without chemical reactions will obtain intact electrode patterns without influence on fabric fibers.[30] Hence, several elements around TMESDs should be taken into consideration, namely, stability of active material,[31] textile-fitting miniaturization technology,[32] and outstanding mechanical reliability of devices.[30]

Serving as one important product with great potential in consumer electronics, flexible wearable equipment is flourishing with the increasing demand and textile-based miniaturized devices.[22] To date, the fabric characteristics and applications are reported as a starting point in various fields. However, few reviews discuss the application of textiles in microelectronics, especially MESD from the perspective of construction. Herein, we discuss recent advances in wearable TMESDs from the following aspects of device design, techniques fundamental in multiple functional textiles and their emerging applications. Finally, the critical challenges in smart textile devices and systems are elaborated and summarized, also further perspectives are proposed.

2. Device design

The traditional energy storage devices with large size, heavy weight and mechanical inflexibility are difficult to be applied in the high-efficiency and eco-friendly energy conversion system.[33,34] The electrochemical performances of different textile-based energy storage devices are summarized in Table 1. MSC and MB dominate the edge of higher-level integration hence be widely applied in advanced portable devices such as e-skins, smartwatch and flexible touch sensors. Energy density is a core parameter of minimized energy storage devices, which is related to the energy storage mechanism. MB is regarded as the primary choice for minimized powering source due to its adequate energy density and stable voltage output. Generally, MSC shows a better control of rate performance and cycling stability, while it is poor in energy density compared with MB.[35] Herein, small-sized flexible energy storage units satisfy the need for portability well. How to prepare MSCs and MBs with a high specific capacitance/capacity, superior power density, and excellent mechanical reliability is a hot spot for TMESDs.

Corrosive and toxic electrolytes employed in common energy storage devices are accompanied by redundant packaging, which makes it difficult to guarantee mechanical characteristics.[34] To construct flexible MSCs and flexible MBs, researchers have prepared various flexible MSCs and MBs using safe all-solid electrolytes and subsequent packaging processes on various stretched substrates, such as polyimide,[36] polydimethylsiloxane (PDMS),[37] tantalum (Ta),[38] titanium (Ti),[39] wood-based,[40] mica-based[41] and paper-based[42] materials. The rich porous textile-based substrate is attracting much attention due to its unique mechanical flexibility, high surface area and lightweight.[43] The developed configuration of MESDs generally includes thin-film MESDs,[44] interdigital MESDs[27] and fiber-shaped MESDs.[10] Here, the distinctive advantages of the three

Table 1 Electrochemical performances of textile-based energy storage devices

Cathode//anode materials	Device type	Power density	Energy density	Specific capacitance/ capacity	Capacitance/ capacity retention under stress	Ref.
$Co(OH)_2$@NiCo LDH//Zn	Microbattery	14.4 mW cm^{-2}	0.17 mW h cm^{-2}	0.44 mA h cm^{-2}	93.6% after 2000 cycles	27
Ni–Co bimetallic oxyhydroxide//Zn	Microbattery	10.3 kW kg^{-1}	256.2 W h kg^{-1}	0.36 mA h cm^{-2}	90.6% after 1600 cycles	19
rGO//rGO	Microsupercapacitor	2.51 mW cm^{-2}	0.00051 mW h cm^{-2}	8.19 mF cm^{-2}	97.2% after 2000 cycles	16
MnO_2/Ag	Microsupercapacitor	500.95 W kg^{-1}	17.5 W h kg^{-1}	46.6 mF cm^{-2}	86.8% after 1000 cycles	45
MnO_2/CNT//V_2O_5/CNT	Asymmetric microsupercapacitor	0.63 mW cm^{-2}	0.00088 mW h cm^{-2}	2.67 mF cm^{-2}	—	46
Poly(3,4-ethylenedioxythiophene) coated titanium oxynitride//vanadium nitride	Asymmetric microsupercapacitor	45 mW cm^{-2}	0.0324 mW h cm^{-2}	72 mF cm^{-2}	—	47
rGO-Ni//rGO-Ni	Supercapacitor	1.86 mW cm^{-2}	0.00158 mW h cm^{-2}	72.1 mF cm^{-2}	100% after 1000 cycles	10
Ni–NiO//Zn	Fiber-shaped battery	20.2 mW cm^{-2}	0.0066 mW h cm^{-2}	0.23 mA h cm^{-3}	—	48
PEDOT:PSS//PEDOT:PSS	Fiber-shaped supercapacitor	3.52 mW cm^{-2}	0.041 mW h cm^{-2}	93.1 mF cm^{-2}	94% after 200 cycles	49
Polypyrrole/rGO/$SnCl_2$ modified polyester yarn	Supercapacitor	26.5 mW cm^{-2}	0.0472 mW h cm^{-2}	339.7 mF cm^{-2}	98.3% after 1000 cycles	8
Polyaniline/rGO/polyester	Supercapacitor	0.807 mW cm^{-2}	0.054 mW h cm^{-2}	781 mF cm^{-2}	95.6% after 1000 cycles	11
Graphene nanopetals/ carbon fiber tow//MnO_2/ buckypaper	Supercapacitor	15.4 mW cm^{-2}	0.050 mW h cm^{-2}	163.5 mF cm^{-2}	93% after 100 cycles	50
Hollow rGO/PEDOT:PSS	Supercapacitor	0.0665 mW cm^{-2}	0.0271 mW h cm^{-2}	304.5 mF cm^{-2}	—	51
CNT/MnO_2 fiber//CNT/ polypyrrole film	Supercapacitor	—	0.0189 mW h cm^{-2}	60.43 mF cm^{-2}	80% after 5000 cycles	52

configuration modes on TMESDs will be reviewed and summarized.

2.1 Construction of thin-film MESDs

MBs and MSCs with the sandwiched structure are assembled by the separator face to face through two electrodes with the electrolyte and subsequent packaging. Limited by the stability of the microelectrode with high loading of active materials, MESDs with thin-film form are greatly developed, and the related high volumetric utilization is thoroughly studied from the perspective of material designs.

As far as the substrate is concerned, flexible substrates used in the construction of thin-film MESDs can be roughly divided into two types: non-conductive substrates and conductive substrates. The commercial fabrics of the former type show great promise for their low cost and easy access. However, the use of non-conductive materials as a substrate requires the addition of other functional additives such as conductive agents and active materials. Herein, Tong *et al.*[44] reported a stretchable Ni@NiCoP coated spandex with excellent electrical conductivity. In this work, commercial spandex obtained directly by cutting clothes is applied as a flexible substrate, and a nickel (Ni) layer was coated on the substrate by polymer-assisted metal deposition (PAMD). Then, the obtained Ni-coated spandex-textile (Ni ST) was immersed in an electroless deposition bath and heated at 90 °C for 15 minutes, followed by cleaning and drying Ni@NiCoP ST. Ni@NiCoP@single-wall carbon nanotubes (SWCNT) ST were obtained afterward by putting Ni@NiCoP ST into SWCNT ink and drying several times in an electric oven. The asymmetric supercapacitor (ASC) showed an ideal areal capacitance of 877.6 mF cm^{-2}, and desirable capacitance retention of 98% for 6000 cycles (at 100 mV s^{-1}). Furthermore, Chen *et al.*[53] electrodeposited Ni–Al layered double hydroxide (LDH) nanoparticles with low crystallinity onto a Ni-coated cotton textile (NCT) through a combination of electrodeposition and electroless plating of Ni. NCT@NiAl-LDH, NCT@G-Fe_2O_3, and polyvinyl alcohol (PVA)/KOH were used as the anode, cathode and gel electrolyte, respectively. The prepared wearable ASC has a high specific energy density of 58.8 W h kg^{-1} (134 μW h cm^{-2}) when the specific power density is 539 W kg^{-1} (1228 μW cm^{-2}).

In addition to using transition metal elements as active conductive materials, MXene, a new 2D material, with superior hydrophilicity and high electrical conductivity, showed great potential in electrochemical devices. MXene has high toughness and the edges of the layered sheet provide higher electrochemical mechanical support, showing enough strength for flexible wearable devices.[54] Ma and co-workers[55] reported

a polypyrrole (PPy)-MXene-coated cotton textile. In that work, they coated MXene on the surface of the cotton fabric with abundant hydrophilic groups through the facile surface dipping method, and then PPy was electroplated onto the surface of MXene-based textile using an electroplating system. With the H_2SO_4/PVA gel electrolyte, the MXene-PPy textile electrode delivered a specific capacitance of 182.70 F g^{-1}. To prepare wearable energy fabrics that adapt to the motion of a human joints, Kim *et al.*[14] reported an electrochemical SC that can withstand all-around deformation. As shown in Fig. 1a and b, multi-walled carbon nanotubes (MWCNTs) were dispersed in sodium dodecylbenzene sulfonate (SDBS) as a surfactant to prepare aqueous CNT ink. Subsequently, polyurethane and polyester copolymer were immersed in the CNT ink for 10 minutes, and the CNT-coated textile was obtained from drying–washing–drying. After the reaction in a water bath, the conductive polymer (polyaniline, PANI) layers can be polymerized *in situ* on CNT/textile. In detail, PVA/H_3PO_4 aqueous gel electrolyte is sandwiched between two PANI/CNT/textile electrodes to make a symmetrical SC. Owing to the redox activity of the PANI layer, PANI/CNT/textile-capacitor showed a larger inner area of the CV curve than CNT/textile capacitor (Fig. 1c). Fig. 1e is a schematic of the omnidirectional stretchability of the PANI/CNT/textile capacitor. Under various omnidirectional stretching levels, the capacitor delivered stable energy and high-power densities (Fig. 1f and i). The symmetrical SC delivered an excellent specific capacitance of 412 mF cm^{-2} (Fig. 1d), a capacitance retention of 95% (Fig. 1g), and high cycling stability (>2000 times stretches) (Fig. 1h). Moreover, under the dynamic deformation cycles, LED maintained a stable brightness as shown in Fig. 1j.

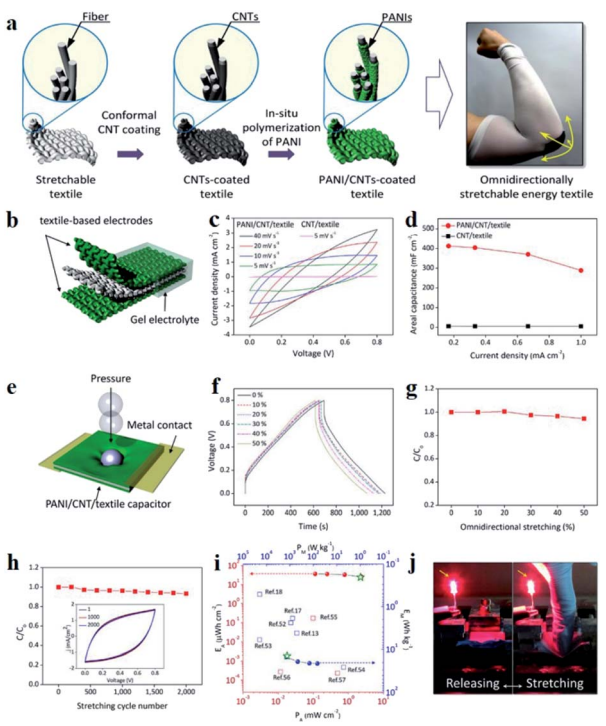

Fig. 1 (a) Synthetic procedure of PANI/CNT. (b) Device configuration of electrochemical capacitors assembled from the textile-based electrode and gel electrolyte. (c) Cyclic voltammetry curves of textile-based electrochemical capacitors under different scan rates. (d) Areal-specific capacitance *vs.* current density. (e) Schematic illustration of evaluation method for omnidirectional stretchability of PANI/CNT/textile capacitor. (f) Galvanostatic charge/discharge curves at various omnidirectional stretching levels. (g) Capacitance retention under omnidirectional stretching levels. (h) Cycle stability of PANI/CNT/textile capacitors under repeated 20% omnidirectional stretching level. (i) Ragone plot with the previously reported stretchable electrochemical capacitors. (j) LED lighting powered by PANI/CNT/textile capacitors under finger pressure. Reproduced with permission.[14] Copyright 2019, American Chemical Society.

However, it is unavoidable that the space available for active material will significantly decreased due to the presence of the non-conductive fabric. The use of conductive substances, such as CNT,[56] carbon cloth (CC),[33,57,58] and carbon fiber (CF)[59] is also an indispensable way to improve the utilization of active materials. In research on these conductive carbon-based substrates, commercial CC is the most commonly used conductive substrates. Cao *et al.*[57] reported a N/O-enriched CC with a porous structure and used the modified CC as an electrode to prepare a symmetric SC. The effective textile process combining wet-spinning with KOH activation endowed N/O-enriched to carbon microfiber cloth with excellent mechanical performance. Then, C, N, O functional groups such as C–O were introduced on N/O-enriched CC through electrochemical oxidation for 3 minutes. The high surface area of modified CC allowed a large amount of charge to interact through the interface of electrode/electrolyte. Moreover, functional groups rich in N/O directly participate during the redox reaction, such that the modified CC exhibited significant pseudo-capacitance characteristics. The symmetric SC using the PVA/LiCl gel electrolyte and modified CC electrode showed an excellent energy density of 9.4 mW h cm^{-3} and reliable flexibility. In addition, the SC can also power an electronic watch for ~9 h. It is worth noting that the introduction of a large number of oxygen atoms also leads to a decrease in the electrical conductivity of the electrode, which caused a decrease in the rate performance compared with the unmodified CC. For further improving the electrochemical performance of CC textile electrodes, many valuable solutions are proposed. Zhao *et al.*[58] fabricated a commercial CC modified with reduced graphene oxide (rGO) and molybdenum dioxide (MoO_2). In their work, MoO_2 and CC textiles were treated by a solvothermal process for 30 minutes and kept in a Teflon-lined stainless steel autoclave at 180 °C for 6 h. After cleaning and drying, it was annealed in H_2/Ar (v/v: 10%/90%) for 2 h at 450 °C to obtain MoO_2-coated CC textile (MC). Using MC as a filter membrane to filter rGO multiple times can produce rGO-coated MC electrodes. Due to MoO_2 coating, the capacitance and electrical conductivity of CC-based electrodes are improved. In addition to accelerating electron transfer, rGO also prevented MoO_2 from peeling off the carbon fiber, thereby reducing damage to the structure of the electrode during the folding process.

Other than using commercial conductive substrates, converting non-conductive materials into conductive substrates through carbonization is also an effective method for manufacturing TMESDs. Wang *et al.*[60] obtained carbonized silk

cloth (CSCs) through high-temperature treatment of commercially available silk fabrics in Ar/H_2 atmosphere. CSCs were treated with oxygen plasma for 5 minutes to make them hydrophilized, and $Ti_3C_2T_x$ colloidal suspension was slowly dropped on a hot plate at 50 °C to obtain CSC@$Ti_3C_2T_x$ electrodes. The electrode delivered a high areal capacitance of 362 mF cm^{-2} with good flexibility. After the electrodes were coated with PVA/H_2SO_4 electrolyte, two electrodes were assembled face to face to prepare the SC. The CV curve remained almost the same under the straight and bending at 120° under a scan rate of 10 mV s^{-1}. Li and co-workers[61] also prepared cotton T-shirt textiles with high electrical conductivity (sheet resistance of ~10–20 Ω sq^{-1}). Flexible activated carbon textiles (ACTs) were obtained through traditional dipping, drying and curing. The SC using the ACT electrode showed a specific capacitance of 70.2 F g^{-1} at a scan rate of 2 mV s^{-1}.

CNT fabrics have also been widely used in fabric energy storage due to their lightweight and excellent mechanical performance. But the formation of the solid electrolyte interphase (SEI) layer at the CNT fabric surface resulted in a high irreversible capacity (28%). Wu[62] explained that lithium ions can be inserted into the inner core and outer surface of the CNT, while de-insertion can only be performed from the outer surface of the nanotube. Therefore, the deintercalation behavior of lithium ions inserted into the inner core of the nanotube cannot occur, thus contributing to a high irreversible capacity value. Yair *et al.*[56] used different substances to pre-treat CNT fabrics and found that washing with isopropanol leads to bundling and densification of the CNT fabrics. Using isopropanol pretreated CNT fabric as lithium-ion batteries (LIBs) anode resulted in the lowest irreversible capacity (13%). After the isopropanol (IPA) treatment, the CNT film was densified and became thinner, decreasing the amount of irreversible Li-ion insertion, which is beneficial for lowering the irreversible capacity. What is more, coating the active slurry of meso-carbon micro-beads (MCMB) and graphite powder (Targray) on the pre-treated CNT fabric, is an effective way to obtain a high-performance LIB anode.[56]

In addition to extensive research on MSCs in flexible fabric-based energy storage systems, MBs also show great potential in the field of flexible fabric energy storage. Meng *et al.*[33] reported a method that can deposit porous $LiMn_2O_4$ nanowall arrays with three-dimensional (3D) nanostructures on different conductive substrates without using high-temperature processing. In this study, a three-electrode electrochemical cell was used to deposit porous $Mn(OH)_2$ nanowall arrays on a CC substrate through a cathodic deposition, and $Mn(OH)_2$ nanowall arrays could be oxidized to Mn_3O_4 nanowall arrays. $LiMn_2O_4$ nanowall arrays were subsequently prepared using the "hydrothermal lithiation" method. In detail, Mn_3O_4 nanowall arrays were put into LiOH solution and transferred into a Teflon-lined stainless steel autoclave and heated at 240 °C for 17 hours to obtain $LiMn_2O_4$ nanowall arrays. $Li_4Ti_5O_{12}$ nanowall arrays grown on CC textile were also prepared by a solvothermal method, followed by a LiOH lithiation process and high-temperature calcination process.[63] $LiMn_2O_4$ nanowall arrays CC, $Li_4Ti_5O_{12}$ nanowall arrays CC, $LiPF_6$, and Celgard 2400 were used as the cathode, anode, electrolyte and the separator respectively, and then these materials were encapsulated in an Al/polyethylene film to prepare LIBs showing an energy density of 124.8 mA h g^{-1} at 1C (92.1 mA h g^{-1} at 20C) and excellent cycling stability at various bending states.

Thin-film MSCs and MBs with separators are still challenging in precisely regulating the thickness of separators and electrodes, which have a great influence on the degradation of specific capacity.[64] At the same time, there are relatively few reports on textile-based MBs compared to textile-based MSCs because of the lack of suitable active materials. In fact, current battery-active materials have the disadvantage of structural rigidity, which affects their application in wearable devices.[34] Thus, the development of active materials compatible with flexible textile substrates is of great significance to the development of TMESDs.

2.2 Constructing of interdigital MESDs

The in-plane microdevices with interdigital geometry are composed of two adjacent electrodes distributed parallel to the micrometer scale. Contrary to stacked microdevices with low volumetric capacity due to package components, interdigital electrodes with more active loading on every single electrode expose more area in the electrolyte, and no need for separator allows fast-diffusion of ions in the electrolyte and electrode surfaces, which contributes to a specific capacity. The superior rate capability can be achieved by optimizing interdigital electrode architecture with smaller gap distances. To satisfy the requirement of both electrochemical and mechanical characteristics, advanced electrode materials and microfabrication are the keys to flexible MESDs. As the issues of active materials are comprehensively introduced in the subchapter about thin-film MESDs, here we will focus on the specific miniaturization techniques and the corresponding spatial structure for interdigital MESDs, including photolithography and etching methods.

2.2.1 Etching methods. Etching methods including plasma etching and laser etching are widely applied in high-resolution pattern transferred for micro/nanodevices. The process uses physical or chemical methods to sacrifice the part that is without any protection by the mask and leave the desired pattern intact. Among the plentiful varieties, laser engraving technology enables direct patterning to form interdigital electrodes through the thermal effect produced by the laser beam. High-energy laser beam cuts metal locally to carve out the capacitive element for coplanar architecture, in which the parameters such as scanning speed, wavelength and pulse duration can be adjusted to manufacture high-precision microdevices. Jiang and co-workers[65] have successfully achieved 3D current collectors of Ni foam electrodes for MSCs through this method. On the one hand, the intrinsic honeycomb-type microporosity and high electrical conductivity made Ni foam an ideal 3D framework for maximum active loading. On the other hand, a wide temperature range for shape preservation and stable chemical environment of Ni foam facilitated laser machining and subsequent fabrication process for carbon nanofibers as a negative electrode. Laser processing is a better choice for wearable microelectronics due to its

applicability to flexible media. Through contact-free and facile pathways, laser engraving enables patterning for flexible microelectrodes arrays and cutting into planar geometries. In view of this, Wang and co-workers[27] fabricated a wearable textile-based Co–Zn alkaline MB with trench-type configuration, where, the laser engraving method was used for cutting hierarchical $Co(OH)_2$@NiCo-layered double hydroxide@Ni-coated textile (CH@NC-LDH@NT) core–shell architecture and Zn@CC into individual microelectrodes. The fabrication process of Co–Zn alkaline MB is shown in Fig. 2a. It is noted that the parameters of laser power and cutting speed of Zn@CC need to be decreased due to the flammability of carbon clothes. The subsequently transferred process showed that the interdigital CH@NC-LDH@NT cathode and Zn@CC anode obtained using direct laser engraving process could be properly placed in the corresponding gel electrolyte-filled polydimethylsiloxane (PDMS) based trenches, with intact microelectrodes and no burn marks by a high-energy laser beam. The large potential difference between redox peaks of CV curves (5 mV s^{-1}) of CH@NC-LDH@NT and Zn@CC electrodes indicates that the assembled Co–Zn alkaline MB had a higher output voltage (Fig. 2b) and high electrochemical reversibility (Fig. 2c). Moreover, the characteristic charging and discharging platforms in GCD curves of all MBs near 1.68 and 1.64 V with a small voltage hysteresis ($\approx$0.1 V) are attributed to rapid electron and ion transfer (Fig. 2d). As a result, the assembled flexible Co–Zn alkaline MB showed excellent cycling performance with a capacity retention of 71% after 800 cycles (Fig. 2e), an outstanding areal energy density of 0.17 mW h cm^{-2} (Fig. 2f), and volume energy/power densities of 7.23 mW h cm^{-3}/0.60 mW h cm^{-3} (Fig. 2g). In addition, Tian and co-workers[30] adopted the laser cutting method to fabricate

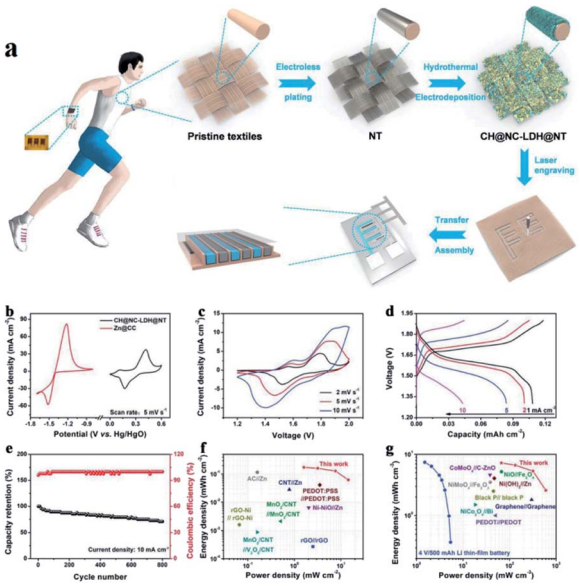

Fig. 2 (a) Fabrication process of Co–Zn alkaline microbattery. (b) Cyclic voltammetry curves of CH@NC-LDH@NT and Zn@CC at 5 mV s^{-1}. (c) Cyclic voltammetry curves, (d) galvanostatic charge/discharge curves, (e) long-term cycling stability, and (f and g) Ragone plots of Co–Zn alkaline MB. Reproduced with permission.[27] Copyright 2020, Wiley-VCH.

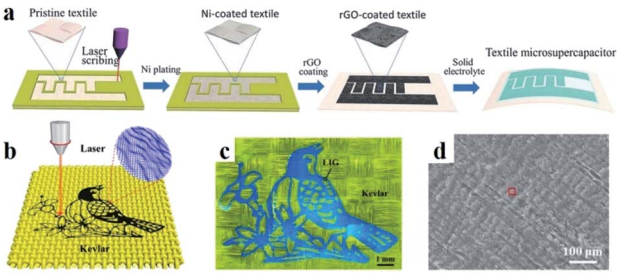

Fig. 3 (a) Fabrication process of textile MSCs. Reproduced with permission.[16] Copyright 2016, Wiley-VCH. (b) Schematic of the graphene/Kevlar textile from Kevlar. (c) SEM image of laser-induced graphene (LIG) on a Kevlar textile. (d) SEM image of the LIG circled in (b). Reproduced with permission.[18] Copyright 2020, American Chemical Society.

flexible alkaline micro zinc ion battery (ZIB) arrays with favorable rate performances. They carved foiled zinc anode and free-standing layer double hydroxide (LDH) cathode into various planar shapes and assembled them into micro-ZIB. The interdigital electrodes with an approximately 1 mm gap distance and neat edges resulted in a mature control of accuracy for the high-energy laser beam. After the laser-assisted process, by covering plastic films as a capping layer and filling PVA as an electrolyte, the obtained micro ZIB exhibited remarkable flexibility. Moreover, Pu *et al.*[16] developed a laser-scribing masking route to produce textile with customizable patterns, as shown in Fig. 3a. Graphene is favored by flexible electronics due to its inherent mechanical strength and electrical conductivity, which can be well transferred to any ideal substrate after etching the metal.[66] Wang and co-workers[18] demonstrated direct writing of laser-induced graphene (LIG) on Kevlar textile, as shown in Fig. 3b and c. SEM image showed that the fabricated LIG had a porous morphology and nano-shaped ripples (Fig. 3d). El-Kady *et al.*[67] demonstrated a scalable fabrication of graphene MSCs *via* direct laser writing on GO films. They found that laser-induced expansion of the film ameliorates the electrode surface, which demonstrated a power density of ~200 W cm^{-3}. For graphene by chemical vapor deposition (CVD), laser treatment enables selective control of layer thickness and mask-free patterning. By patterning 3D graphene/Kapton assembly *via* laser machining, Zhang *et al.*[68] prepared interdigital electrodes and assembled flexible monolithic 3D graphene MSCs with high power density. The rapid heat dissipation of the high-energy laser beam realized selective etching on CVD-made 3D graphene. Furthermore, Ye *et al.*[69] reported a flexible solid-state MSCs based on CVD graphene films performed desirably in both hydrogel and ion-gel electrolytes. The laser fabrication technically facilitates structuring and patterning, thereby demonstrating advancements in highly integrated MSCs.

To sum up, the laser engraving technology has a high universality in the micromachining of wearable flexible MESDs, which shows the following significant predominance: firstly, the laser-cut process displays ultrahigh precision and machinability owing to the small light spot and high energy density of laser; secondly, the microelectrode morphology can be customized to have a range of versatility to the microdevices;

finally, the laser engraving technology perfectly coordinates subsequent processes to impart outstanding electrochemical properties and flexibility to the devices.

After it became mature etching technology in the 1980s, plasma etching has gone through more than 40 years of development for integrated circuits. Serving as an indispensable link in the manufacture of microelectrodes array, it removed portions that were uncovered by the deposited film through plasma reaction. The active carbon-based film with outstanding electric conductivity, high specific surface area and applicability to a variety of flexible substrates, can coordinate with plasma-etching technology to fabricate microelectrodes for flexible MESDs.[70,71] In 2014, Wu *et al.*[72] deposited Au current collector onto a patterned boron co-doped graphene (BNG) film, and next used oxygen plasma etching to remove exposed graphene area. After drop-casting and solidification of the gel electrolyte, they obtained BNG-MSCs providing an ultrahigh volumetric capacitance of ~488 F cm^{-3}. In 2015, Liu *et al.*[73] utilized the thermal evaporation method to grow gold layer onto the as-prepared graphene oxide (GO)/manganese dioxide (MnO_2)/silver nanowire (AgNW) (GMA) ternary hybrid film. Through oxygen plasma etching of exposed GO, the patterns of GMA microelectrodes were then created on an alumina substrate. After cleaning with HCl and thermal-reduction process, the binder-free microelectrode was obtained for reduced GMA (RGMA) MSCs with robust rate capability of up to 50 000 mV s^{-1} and excellent stability of 90.3% initial capacitance after 6000 cycles. Besides, the electrochemical properties of RGMA MSCs were hardly affected at different angles of bending, which showed the sustainable flexibility of the RGMA ternary hybrid film that can be applied to LIBs.

However, in the photolithography process that matched with the etching, carbon-based films can be easily contaminated by photoresists due to their active surface and microporous network structure, thus resulting in a serious blow to electrical properties. To date, one-step mask-free plasma etching has gradually developed into a feasible strategy for planar interdigital microelectrode. Herein, Liu *et al.*[70] reported a mask-free micro-plasma-jet etching method to fabricate MWCNTs electrodes for all-solid-state flexible MSCs. Atmospheric pulsed micro-plasma-jet (APMPJ) directly scanned CNT films into interdigital electrodes with no need for photolithography, so as to give full play to the capacitance and flexibility of the fabricated MSC. Liu *et al.*[71] adopted a similar method to obtain interdigital MWCNT/AgNW electrodes for all-solid-state flexible in-plane MSCs. The ejected electric charges in plasma contacted the MWCNT/AgNW film generated Joule heat, which etched both MWCNTs and AgNWs. Compared to the traditional plasma etching process, APMPJ put aside the tedious fabrication and high concentration of O_3 distinctly facilitated the etching of MWCNT in the interspaces, which provided effective separators between interdigital electrodes beneficial to the rate capability. For fabric substrates, plasma treatment can be used to improve surface conditions such as hydrophilic or hydrophobic properties. In this direction, Kan *et al.*[74] regulated the wettability of polyamide and polyester fabrics by forming polar groups on the surface. Li *et al.*[75] proposed a novel method that combined plasma etching and fluoropolymer deposition to alter the average size and interspacing of fibers so as to create a superamphiphobic cellulose-based paper substrate. By selectively etching with an oxygen plasma and followed by fluoropolymer coating *via* plasma-assisted deposition, superhydrophobic and superoleophobic nature that is suitable for wearable fabric was thus desirably achieved.

Microfluidic etching is a tactile and high-precision pattern transfer method for on-chip microdevices based on microfluidic technology. The upper and lower layers constitute the main body of the microfluidic chip, in which PDMS is commonly acting as an impression layer for high elasticity and favorable light transmittance. Etchant solution instantaneously flows through the microchannel constructed by PDMS and thus achieving micro- or submicron-sized patterns of microelectrodes.[30] Cao and co-workers[76] reported flexible all-solid-state MSCs based on MnO_2 nanoparticles *via* this method. They first prepared nanofiber-based film of MnO_2 through electrospinning, followed by filling of H_3PO_4–polyvinyl alcohol (PVA) gel electrolyte and sputtering of indium tin oxide (ITO) as a current collector. Then, the PDMS layer with a microchannel closely pressured on the MnO_2/ITO film was accompanied by injecting of etchant solution and deionized water. After drying and peeling off the microfluidic PDMS stamp, they finally obtained the flexible MSC, which showed excellent capacitance of 338.1 F g^{-1} and initial capacitance retention of 96% after 500 cycles of charge and discharge at the current density of 2 mA cm^{-2}.

2.2.2 Photolithography. Lithography is a key process for microelectromechanical (MEMS) developed on the basis of photographic technology and planographic printing.[77] Photoresist exhibits corrosion resistance due to the photochemical reaction after exposure, so as to engrave the pattern of the mask onto the processed surface. For scalable fabrication of MSCs and MBs, lithography technology defines the interdigital current collectors in a high-resolution way and provides more creative flexibility for micro/nano energy storage devices. Conventional photolithography is generally followed by a subsequent process such as sputtering, and electrophoretic deposition. For example, Kurra *et al.*[78] fabricated conducting polymer-based flexible MSCs with remarkable performance in energy density and frequency response. The plastic polyehtylenenaphthalate (PEN) was adopted as substrates for interdigital patterning through photolithography and sputtered Au current collector, the porous poly(3,4-ethylenedioxythiophene) (PEDOT) electrode was then grown onto configuration through electrochemical deposition with strong adsorption. Besides, the added sodium dodecyl sulfate (SDS) effectively improved the miscibility of organic electrolytes. The obtained polymer-based MSC exhibited maximum areal cell capacitance of 9 mF cm^{-2} with outstanding capacitance retention up to 80% over 10 000 cycles. He *et al.*[79] designed a microelectrode of carbon microstructure embedded with NiO/Ni nanospheres by combining photolithography with pyrolysis. The MSC delivered a high capacitance of 2.75 mF cm^{-2}. For textile-based materials, light scattering and antireflective properties owing to unique rough surfaces contributes to the

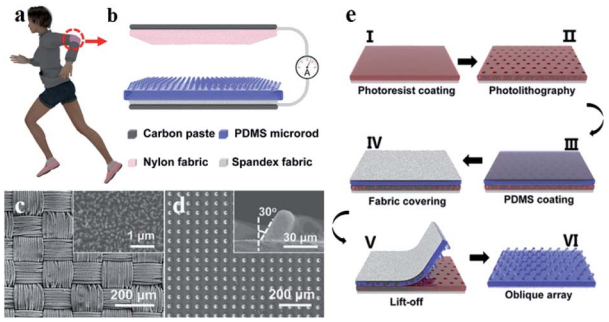

Fig. 4 (a) Schematic of the WTNG sewed on the cloth. (b) The structure design of a WTNG. (c) SEM image of nylon fabric with nanowires. (d) Top-view SEM image of PDMS microrod arrays. (e) The fabrication process of the oblique PDMS microdevices array on a spandex fabric. Reproduced with permission.[81] Copyright 2019, American Chemical Society.

fabrication of textile patterns through photolithography technology. Lim *et al.*[80] reported textile-patterned polydimethylsiloxane (PDMS) film through facile soft imprint lithography, showing improved hydrophobicity and high transparency. In addition, Zhang *et al.*[81] employed an oblique microrod array to fabricate a textile-based wearable triboelectric nanogenerator (WTNG). As shown in Fig. 4a and e, the glass substrate with oblique openings worked as a template was prepared by the inclined photolithography. Then, PDMS was used as the imprinted polymer cast on the template and paved a layer of spandex fabric. After the thermal curing process, the oblique textile-based PDMS microrod arrays were successfully obtained. The structure of WTNG was sewed on the cloth as shown in the schematic in Fig. 4b. The nylon fabric woven with fibers showed a diameter of about 10 μm (Fig. 4c) and the oblique PDMS microrod array was distributed regularly on the surface of spandex fabric (Fig. 4d). The novel solution allowed PDMS and flexible fabric to be combined into a unified whole, which can not only withstand high-strength pressure but also ensure the flexibility of the spandex fabric. Besides, the prepared PDMS microrod array contributed more to the output performance of nanogenerators with a maximum peak power density of 211.7 μW cm^{-2}. Furthermore, Li and co-workers[82] demonstrated a flexible pressure sensor based on MXene-textile, in which Mo microelectrode was patterned to interdigitated electrodes *via* photolithography followed by sandwiching the MXene-textile between the polyimide (PI) tape and Mo electrode.

In conclusion, photolithography is the most mature micromachining technology in the field of integrated devices for high-resolution patterning. However, photolithography requires an ultraclean room and the cumbersome technical process such as the liftoff of the photoresist, which obviously restricts the progress in the direct integration of flexible on-chip devices.

2.3 Fiber/yarn-shaped textile-based energy storage device

In addition to the construction methods based on thin-film and interdigital MESDs, fiber/yarn-shaped MESDs are special fabric-based energy storage devices with unique 1D architecture. Compared with planar MBs and MSCs, fiber/yarn-shaped fabric-based batteries exhibit both higher flexibility and air permeability, which can make wearable devices have better comfort and wearing experience.[28,83] Fiber/Yarn-shaped textile-based energy storage device usually uses conductive fibers or non-conductive fibers as the substrate and then deposit electrode materials on the substrate and coat electrolyte. Finally, the two fiber electrodes are placed in parallel or twisted and are encapsulated to prepare fiber/yarn-shaped SCs and batteries. Benefiting from the excellent mechanical performance, inert nature under ambient conditions of CFs, the CF as the substrate of fiber/yarn-shaped textile-based energy storage device has received much research interest. Chen *et al.*[83] synthesized activated carbon coated carbon fibers as a yarn SC electrode. In this work, a high-viscosity activated carbon suspension was directly coated on the CF and was twisted using a handheld yarn spinner. The electrodes were dried in a vacuum oven for 8 hours, then immersed in polyvinyl alcohol (PVA)/H_3PO_4 electrolyte for 20 minutes and dried at room temperature. Among them, PVA/H_3PO_4 served as both the electrolyte and the separator of the two electrodes of the yarn SC. The activated carbon was not only coated on the surface of the CF but also filled in the gaps in multiple CFs. The prepared SC showed an energy density of 6.5 mW h cm^{-1} and a power density of 27.5 mW cm^{-1}. Even at a power density of 220 mW h cm^{-1}, it still showed an energy density of 3.0 mW h cm^{-1}. When the length was 50 cm, there was a high capacitance of 1164 mF. Due to the excellent energy storage capacity of transition metal oxides and conductive polymers, they are widely used in fiber/yarn-shaped energy storage devices to improve the performance of yarn MSCs and MBs. Wang *et al.*[84] loaded poly(3,4-ethylenedioxythiophene)–poly-(styrene sulfonate) (PEDOT:PSS) on carbon nanofiber (CNF)-coated CF bundle. CNF ink was coated on CF by heat treatment in the oven at 100 °C for 15 min after drop casting. PEDOT:PSS was drop-coated on the carbon fibers, followed by annealing at 120 °C on the carbon. In order to increase the loading of CNF and PEDOT:PSS, the process can be repeated several times. The yarn-shaped SC was obtained by coating the two electrodes with PVA/H_3PO_4 electrolyte and placing them in parallel. The group also deposited $RuO_2 \cdot Th_2O$ on CFs by a vapor-phase hydrothermal method[13] as shown in Fig. 5a, and immersed it in the PVA/H_3PO_4 solution as electrodes for 10 minutes, keeping the two ends above the solution. The two fibers were assembled into a copper-clad EVA tube covered by PDMS, separated by a paper separator, and the exposed part was reserved as an electrode terminal. Fig. 5b shows a single fiber-shaped supercapacitor (F-SC), and the carbon exhibited excellent chemical stability and conductivity. Moreover, several CFs were assembled into a bundle coated with $RuO_2 \cdot xH_2O$ (Fig. 5c and d). According to the equation $E = 0.5CV^2$, two electrodes with different working potentials can be used to broaden the working potential window of MSCs and MBs to increase the energy density. The CV curves (Fig. 5e) of F-SC without significant distort and the charge/discharge curves (Fig. 5f) with no obvious *IR*-drop phenomenon reconfirmed the excellent capacitive behavior of F-SC. Furthermore, the F-SC has a stable cycling performance after 5000 cycles under the current

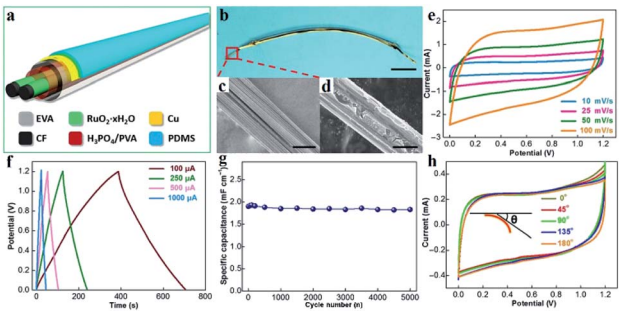

Fig. 5 (a) Schematic and (b) photograph of a single F-SC consisting of two carbon fibers coated with $RuO_2{\cdot}xH_2O$ in the electrolyte. (c) Low-magnification and (d) high-magnification SEM image of the carbon fiber electrode. (e) CV curve of the single F-SC at various scanning rates. (f) Galvanostatic charge/discharge curves of a single F-SC at different current densities. (g) Cycling stability of a single F-SC. (h) CV curve of the single F-SC at different bending angles. Reproduced with permission.[13] Copyright 2016, the American Association for the Advancement of Science.

of 1000 μA and reliable energy storage at various bending conditions (Fig. 5g and h). Huang and co-workers[76] used $NiCo_2O_4$ nanograss-coated CF ($NiCo_2O_4$NG@CF) (derived by a hydrothermal method and subsequent annealing in N_2 atmosphere) as cathode, and porous carbon coated-CF, which was derived from lemon peels by hydrothermal carbonization combined with 20% KOH activation as the anode of the yarn SC, to assemble an SC. The prepared HSC showed maximum-specific capacitance of 17.5 F g^{-1} (25.03 mF cm^{-2}) at a current of 1 mA, and an energy density of 6.61 W h kg^{-1} (9.46 mW h cm^{-2}). Among conductive carbon materials, CNT is a potential substrates and active materials in fiber/yarn-shaped textile-based energy storage devices due to its excellent tensile strength (500–800 MPa)[28] and electrical conductivity. Kim *et al.*[85] used polyurethane-coated CNT yarns directly as SC electrodes and wound them on silicone rubber fiber. Then it was inserted into a silicone rubber fiber with a large inner diameter, and 10 wt% PVA in 0.1 M HCl solid electrolyte was injected. The solid-state yarn energy harvester was also manufactured using the same method, except that the CNT yarns were different (when stretching the harvester, homochiral CNT yarn was twisted, and heterochiral CNT yarn was untwisted), and these two systems could also be integrated into one wearable device. In order to further enhance the performance of the yarn SC, Miao and colleagues[28] deposited conducting polyaniline (PANI) nanowire *in situ* arrays on the CNT yarn through a dilute polymerization process as the electrode of the yarn SC. Since the coating of PANI leads to lower electrical conductivity of PANI-coated CNT than that of the original CNT yarn electrode, the areal capacitance of the PANI-coated CNT yarn electrode will decrease rapidly when the current density increases.

Similar to TMESDs constructed in a flat plane, in order to reduce production costs as much as possible, non-conductive polymer fiber-based MESDs are also very important in the research of TMESDs. However, in order to improve the electrical conductivity of non-conductive substrate, a layer of highly conductive material needs to be coated on the surface. Wang *et al.*[10] used electroless plating to deposit Ni metal on a polyester yarn with 500 μm diameter to make it highly conductive (1.48 Ω cm^{-1}). Then, the Ni-coated polyester yarns were immersed in the GO dispersion for 6 hours of hydrothermal reaction at 80 °C. Finally, the yarns with spontaneously formed rGO hydrogel film were further reduced in a 0.1 M ascorbic acid at 90 °C. The fabricated all-solid symmetrical SC was assembled using two rGO-Ni-yarns and PVA/H_3PO_4 electrolytes. Under the synergistic effect of Ni and rGO, SC showed capacitance of 13.0 mF cm^{-1} (72.1 mF cm^{-2}) and stable cycling performance (96% for 10 000 cycles). What is more, there was no significant drop in performance after 1000 cycles.

Fiber/yarn-type MESDs could be easily integrated with other devices through textile technology to solve the problems in wearable manufacturing. The capacitance of the yarn MSCs and MBs is largely determined by the length of the yarn electrode. However, the longer the length of the yarn SC or MB means the greater the resistance, which reduces their rate performance.[10] Therefore, the development of fiber materials with high conductivity, high flexibility, lightweight, and low cost is also a very important work in TMESDs.

3. Technique fundamental

Serving as a flexible functional material, three routes are followed for attaching the electronic function to textiles. The first route is designing nanostructure fiber with electronic properties, which optimize the morphology and homogeneity of the as-prepared fibers simultaneously on a micro-level, using processing techniques such as spinning. The second one is constructing a conductive medium on the surface of the wearables with the help of coating and printing techniques. This way could achieve the scalable and simple production process of MESDs. The third route is integrating microelectronic devices into the knitted functionalized fabrics, fibers, or yarns. The unique ultralong 1D textile structure improves electronic transport and thus plays a better synergistic role with loading equipment.

3.1 Coating strategy

Building a conductive layer on the surface of textile, yarn or fiber can meet the electrical requirements of microelectronic devices without altering the inherent properties of textiles, such as flexibility and durability. Currently, feasible manufacturing methods include dip coating, printing technique, and deposition methods, *etc.*

Dip-coating is a simple process for preparing a thin and uniform functional coating onto various substrates, in which the substrate is fully dipped into the precursor solution and then slowly be removed from the solution, and the redundant was removed after a few seconds. Liu *et al.*[86] dipped pretreated poly (ethylene terephthalate) (PET) textiles into $Ti_3C_2T_x$ MXene solution, enabling strong interaction between the MXene and textiles, therefore endowing a better control of both flexibility and energy conversion of textile substrates. In addition, Liu *et al.*[12] dipped aqueous GO dispersion onto the surface of

cellulose fibers paper and then reduced it by hydrazine monohydrate to fabricate rGO/cellulose fibers composite paper. Porous cellulose fiber network in nanostructured rGO composite paper not only guarantee fast electrons transport but also alleviated the aggregation of rGO sheets and promoted the penetration of liquid, showing broad prospect for flexible and foldable SCs. Despite the simple operation, variable factors such as the solution concentration, pulling speed and drying conditions limit their high-precision preparation.

Printing techniques can accurately regulate the position of the pattern on the devices. It is noted that the rough and porous structure of textiles makes the functional materials trapped and thus leads to low spatial resolution and poor conductivity of devices.[87] Therefore, in addition to simplifying the manufacturing processes, it is also a challenge to design and optimize the conductive inks for printing. The printing technologies applied to textiles include screen printing, inkjet printing and 3D printing. Screen printing has been used for the construction of MESDs due to its cost-effectiveness, mass-production and easy processing.[88] The method with high throughput can precisely control the spatial resolution by coating the target materials on a stencil-covered substrate.[32] Through the methodology of screen-printing and electrospinning, Cao *et al.*[89] fabricated a self-powered nanofiber-based triboelectric sensor (SNTS) assembled by nanofiber membrane and Ag nanoparticle electrode. The screen-printed Ag nanoparticles (AgNPs) built a strong conductive network, which provided support for the fantastic conductivity and breathability of the electrode. To date, graphene textile electrodes are widely applied to wearable devices for their flexibility and washability. By coating the graphene flakes, Xu *et al.*[90] designed a dry electrode for electrocardiogram (ECG) monitoring based on cotton fabric *via* screen printing, indicating a low sheet resistance of 42.2 Ω sq^{-1}. The excellent energy storage capacity and solution-processability of MXene make it appropriate as screen-printed ink. Herein, Zheng *et al.*[91] reported multitasking MXene inks for high-performance MESDs. The highly elastic rheological properties of MXene inks presented clear and non-short-circuit printed architecture, which is attached to the fabric substrate in a versatile manner for all-flexible self-powered systems. Different from the complicated processing steps and ink waste in screen-printing, inkjet printing only needs low volume of functional material in diluted ink and is able to deposit conductive or functional layers on a target region of the substrate.[92] Modular printing without any tedious procedure is a highlight of inkjet printing. Cheng *et al.*[93] reported flexible planar MSCs with porous nanofibers-like electrodes through inkjet printing. Ag inks were inkjet-printed on preheated terephthalate (PET) for the fabrication of interdigital Ag electrode, in which the heating of the PET substrate contributed to the volatilization of the solvent and the formation of the printed electrode. As mentioned earlier, the rough and porous nature of the fabric affects the permeability and electrical performance of printed ink, which puts forward higher requirements on the particle size and adhesion of inks. Herein, Karim and co-workers[45] reported an organic nanoparticle textile pre-treatment on inkjet-printed graphene-based wearable textiles, which reduced the sheet resistance by three orders of magnitude from 1.09×10^6 Ω sq^{-1} to 2.14×10^3 Ω sq^{-1}. Moreover, Shahariar *et al.*[92] proposed a particle-free reactive Ag ink with inkjet printing on uncoated polyester textile knit, woven, and nonwoven fabrics,

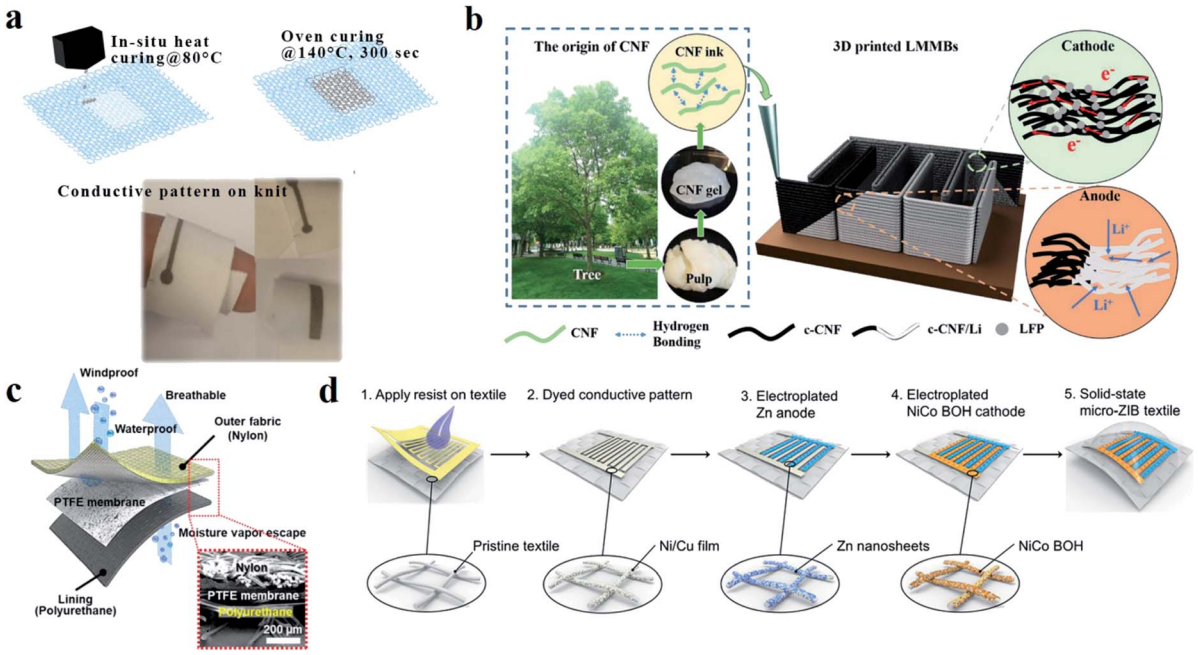

Fig. 6 (a) Systematic process of inkjet printing with reactive Ag ink on textile. Reproduced with permission.[92] Copyright 2019, American Chemical Society. (b) The origin of cellulose nanofiber and fabrication process of 3D printed LMBs. Reproduced with permission.[96] Copyright 2019, Wiley-VCH. (c) Schematic of textile-TENG components. Reproduced with permission.[97] Copyright 2018, Elsevier. (d) Schematic of the fabrication procedures of textile micro-AZB. Reproduced with permission.[98] Copyright 2019, American Chemical Society.

respectively, which could render a conformal coating of conductive network structure on individual fibers without changing the durability and pristine mechanical performance of textiles (Fig. 6a). They also demonstrated that the conductivity and resolution of inkjet printing tracks depended on the tightness and fiber size of the fabrics. Guo *et al.*[94] reported textile-based MSCs with distinct porous structure and rapid electron transport, which combined metal deposition with inkjet printing and extrusion printing. According to the *in situ* cross-linking situation mechanism, the textile was coated with a thin polymer layer and pyridine rings, thereby a highly adhesive alkali-resistant ligand layer was grown, facilitating the subsequent inkjet print-assisted electroless deposition (ELD) of the copper layer. The unique digital patterning capability of inkjet printing not only streamlined the fabrication process but also contributed to the flexibility of MSCs (2000 times@90°), which can be directly integrated with conductive textiles to support wearable electronics systems. As a result, the porous MSCs delivered an ideal area capacitance (8.8 mF cm^{-2}@0.5 mA cm^{-2}, 1.0 mF cm^{-2}@5 mF cm^{-2}) and cycle life of more than 6000 times. In conclusion, inkjet printing has obvious advantages of non-contact and ink saving. The challenge now focuses on the controllable stability of ink and ion diffusion efficiency of the printed electroactive surface.[95]

As a revolutionary manufacturing technology, 3D printing has penetrated into all aspects of modern production. The technology provides customized integration strategy of forming powdered raw materials through layer-by-layer stacking. The rapid conversion from the blueprint to the entity opened up the exploration of 3D printing technology in energy storage material. Compared with planar printing, it allows integrated molding of the electrode and other components. Moreover, controllable thickness effectively improves areal capacitance, which provides a facile way for constructing microelectrode and subsequent encapsulation of minimized devices.[99] The inks for 3D printing need high viscosity and shear-thinning behavior. To date, the representative works in 3D printing concentrate more on lithium-ion MBs, while scarcely on lithium metal MBs (LMBs) due to difficulties in printing lithium metal. As one of the most earth-abundant biopolymers, the cellulose nanofiber has unique shear properties in printing inks, which resulted from its rich hydroxyl groups. Cao and co-workers[96] fabricated LMBs on the basis of cellulose nanofibers for the first time. The origin of cellulose nanofiber and the fabrication process is shown in Fig. 6b. In this work, they used an extrusion-based 3D printing technique to fabricate the cellulose nanofiber scaffold, and then infused lithium metal into the carbonized scaffold to form the anode with a high aspect ratio. The porous structures improved ion transport, and proper pore size allowed lithium-ion to be deposited and remain confined, which prevented lithium dendrite growth. After full assembly, the 3D-printed MBs exhibited a high capacity of 80 mA h g^{-1} at a charge/discharge rate of 10C with capacity retention of 85% even after 3000 cycles. Polydimethylsiloxane (PDMS) has excellent stability and stretchability in flexible devices while being restricted in 3D printing because of the low viscosity.[100] To overcome the problem, Chen and co-workers[16] developed a direct-ink-writing (DIW) 3D printing to prepare coaxial stretchable fibers based on PDMS. By filling polytetrafluoroethylene (PTFE) particles in insulative sheath and graphene in the conductive core, the rheological properties of PDMS pre-polymer were obviously optimized including fluidity (before molding) and rapid solidification (after molding) to meet the requirement of 3D printing. Additionally, PTFE significantly increased the electronegativity in favor of the triboelectric effect. Accordingly, the 3D printed smart textiles achieved excellent performance for tactile sensing and flexibility, which had great potential for e-skin and wearable microelectronics. However, high cost and complicated post-processing limit the utilization of 3D printing, which proposes a trend of combining other assisted techniques such as the introduction of the ultrasonic atomizing nozzle.[99] For flexible devices, mechanical performance related to the life span also needs to be discussed for ever-developing 3D printing technology.

Various deposition methods based on dry fabrication of conductive materials have been widely used for conductive materials. Sputtering is a common physical vapor deposition (PVD) technology for electrode making, which can precisely control the film thickness of sputtered material compared to solution-based coatings. In the process of sputtering, the target metal is bombarded with highly energetic ions at elevated working pressure, which then forms nanoparticles and deposits on the substrate.[101] Kim and co-workers[102] demonstrated a 3D flexible Li-ion MB *via* microcontact printing (μ-cp) and radio frequency (RF) magnetron sputtering. They chose transparent poly(ethylene naphthalate) (PEN) as a flexible and chemically stable substrate to fabricate graphite/silicon hybrid electrodes. The sputtered 3D-structural thin copper serving as a current collector, improved synergistic merits for both graphite and silicon, resulting in a high-rate capability for LIB. Furthermore, Kim *et al.*[97] used woven textiles as a flexible component to fabricate cost-effective wearable and breathable flexible triboelectric nanogenerators (TENGs) by electron-beam sputtering on a polyurethane surface. As shown in Fig. 6c, they built droplet-like islands morphology of deposited Au and delivered an efficient metal-mask for the next plasma-etching process on a woven fabric surface for the effective harvest of triboelectric energy. He *et al.*[103] provided a facile electrochemical deposition to achieve a short transport path of ion and high feasibility. They deposited Bi anode and $Ni_{1-x}Co_x(OH)_2$ cathode on a Cr/Au interdigital current collector, which was made of a liftoff technique, achieving fine interdigital microelectrodes with better control of shape and gap. The fabricated Ni//Bi MB showed an excellent energy density of 12.3 μW h cm^{-2} and desirable stability of 84.44% capacity retention after 1000 cycles. Metallic lithium has the prominent characteristic of highest theoretical capacity (3860 mA h g^{-1}) and lowest electrochemical potential (−3.04 V *versus* the standard hydrogen electrode) while restricted to the utilization of Li-metal anodes because of dendritic Li, which may puncture battery separator leading to inevitable failure.[104–106] The construction of 3D conductive scaffolds can control the nucleation process in lithium deposition by providing active sites, thereby almost avoiding this problem. Here, Wang *et al.*[107] reported a well-designed two-stage

"outside-in" Li deposition based on the hierarchical porosity of bio-derived hollow carbon fiber textiles. Different from the randomness of Li deposition caused by the lipophobic property of carbon-based material,[108,109] they prepared highly porous hollow carbon fiber textile (HPHCT) with crafted dimensions and topologies within the fiber to control the order of deposition. The carbon fibers of HPHCT showed a unique hollow morphology with an ion transfer pathway after the activation process. As a result, Li uniformly and stably deposited on the porous external surface at first, followed by both inside and on the wall of the hollow carbon fiber. The obtained Li composite anode eventually showed a high coulombic efficiency for more than 500 cycles and high cycling stability of over 1400 h at a current density of 1 mA cm^{-2}. Asymmetric MSCs (A-MSCs) are a competitive choice to obtain desirable power density with the assistance of the positive and negative electrodes. Herein, He and co-workers[110] reported a planar A-MSC *via* a facile one-step electrodeposition method to fabricate the cathode of Mn_x-$Co_{1-x}(OH)_2$. Mn–Co–H nanosheet arrays were uniformly deposited on a microscale current collector with networking structure. At the same time, transition metal hydroxides with high ionic diffusion and electrical conductivity effectively enhanced the areal capacitance of electrodeposited Mn–Co–H. The fabricated A-MSC exhibited a high specific capacitance of 32 mC cm^{-2} and an excellent energy density of 7.78 μW h cm^{-2}. In short, the sputtering process allows a variety of substances to be deposited on the substrate stably and uniformly without chemical reactions, while there still exist disadvantages such as poor toughness of the obtained film. Compared with physical vapor deposition (PVD) technology, atomic layer deposition (ALD), as an excellent coating technology, is capable of producing highly pure homogeneous films with well-controlled film thickness as well as conformality to the underlying textile substrate.[111–114] Based on this, Lee *et al.*[115] coated metallic Pt layers by ALD at a low temperature of 80 °C by using [(1,2,5,6-η)-1,5-hexadiene]-dimethyl-platinum(II) (HDMP) and O_2 to prepare highly conductive cotton fiber and further fabricated high-performance capacitive textile-based pressure sensor with superior sensitivity and durability under repeated pressures applied for 10 000 cycles. In addition, Marin and co-workers[116] generated conformal zinc oxide films on textiles *via* ALD technology. However, harsh terms such as vacuum operating environment and high temperature extremely limit dry methods in coatings, which need more exploration in this field.

In addition, there are various novel techniques for textile-based coating. Liu *et al.*[19] developed a resist-dyeing process of textile alkaline Zn MBs (micro-AZB) by attaching laser-scribed Kapton film as a resist for subsequent electroless deposition of Ni coating and electrodeposition of Cu coating (Fig. 6d), which showed higher flexibility and better coating-bonding ability of electrodes. Guo and co-workers[117] coated conductive Ni and Cu coatings with arbitrary patterns on fabrics to obtain rechargeable Zn MB with the help of a Chinese traditional Batik wax-dyeing method. In the process of synthesizing conductive patterns on textile, wax serving as an easy-removing resist covered the surfaces, thereby preventing the infiltration of catalyst and metal ions in the premise of maintaining resistance stability of textiles. The obtained in-plane alkaline Zn MB with Zn anode and Ni–Co bimetallic oxyhydroxide cathode achieved an areal capacity of 0.45 mA h cm^{-2}.

3.2 Fiber preparation

The conductive fibers can also be synthesized by adding electrically functional materials into precursors. Currently, the common methods are electrospinning and wet-spinning. Electrospinning is regarded as a simple and effective strategy of continuous functional fiber production. Under high electric potentials, extruded droplets of functional material were stretched because of the electrostatic repulsion within the dispersion and then formed the longer fiber on the substrate. To date, CNFs have been considered as a promising electrode due to their high electric conductivity and large-range stretchability for flexible solid-state SCs. The electrospun polyacrylonitrile (PAN) nanofibrous networks have the advantages of self-standing and ultra-long 1D nanostructures so that can be used for CNF fabrication. Tan *et al.*[20] proposed a convenient one-step strategy that achieved the deposition of magnesium hydroxide ($Mg(OH)_2$) on PAN nanofibers *via* electrospinning. The PAN/$Mg(OH)_2$/*N*,*N*-dimethylformamide (DMF) was electrospun into nanofibers firstly. After carbonization and etching of the MgO template, the flexible freestanding N-doped mesoporous carbon nanofibers (N-MCNF-900) network electrode for the SC was successfully obtained. Scanning electron microscopy (SEM) image showed that electrospun precursor fibers had smooth surfaces with ultrahigh aspect ratio and were well interconnected, which facilitated the subsequent formation of mesoporous nanostructure that offers an efficient pathway for ion/electron transport through carbon network. The obtained SC delivered a remarkable electrochemical performance with an ultrahigh specific capacitance of 327.3 F g^{-1} at a current density of 1.0 A g^{-1} and ultralong cycling stability after 10 000 cycles. Miao *et al.*[118] prepared nitrogen-doped porous carbon nanofibers (NPSCNFs) by electrospinning polyacrylonitrile/polyaniline core–shell composite nanofibers with desirable electrochemical performances. Moreover, Chen *et al.*[119] prepared PAN nanofibers network using PAN solution by electrospinning method, and then carbonized them to obtain CNFs, which are used as the current collector with high electrical conductivity. Electrospinning provides a realistic strategy for enhancing the contact area and sensing the accuracy of sensor textiles as well. Lou *et al.*[21] fabricated polyvinylidene fluoride/silver nanowire nanofibrous membrane (PVDF/Ag NW NFM) and ethylene cellulose NFM (EC NFM) for constructing all-fiber structured pressure sensor textile *via* facile electrospinning technology. By optimizing electrospinning parameters, NFMs exhibited a hierarchically rough structure holding expected sensing capability. The obtained all-fiber sensor eventually performed excellent mechanical stability and was applicable to various real-time pulse monitoring. Furthermore, electrospun nanofibers can be directly polarized under a strong electric field, which makes sense in piezoelectric power generator fabrication. Lin and co-workers[122] prepared core–shell nanofibers mats of PDMS ion gel/PVDF-HFP *via* coaxial electrospinning. The polyvinylidene fluoride–hexafluoro propylene (PVDF–HFP) shell

coordinated with 3D network polydimethylsiloxane (PDMS), so as to apply to both tactile pressure sensor and triboelectric nanogenerator. Considering the industrial application of electrospinning, the nozzle-receiving device and auxiliary electrode can be improved for the preparation of oriented fibers.

Wet-spinning, as a mature technology that converts polymer solutions into gel-fibers and solid fibers through coagulation, has been widely used to prepare conductive fibers. Wang *et al.*[123] successfully achieved conductive hollow AgNW–CNF fibers by loading AgNWs into renewable cellulose nanofibers *via* wet-spinning, which could be assembled into a textile material as flexible conductors with high conductivity of 6.8×10^5 S m^{-1}. MXene is an ideal choice for fiber making due to its attractive metallic conductivity. Herein, Seyedin *et al.*[120] utilized a scalable wet-spinning technique to produce MXene/polyurethane (PU) composite fibers with superior stretchability and conductivity (Fig. 7a), which can be further applied to strain sensors. Fig. 7b demonstrates that about 100 meters of fibers are continuously collected on the spool under the MXene loading of ~9.1 wt%. Han and co-workers[124] reported an additive/binder-free entirely pure MXene fiber with ultrahigh electrical conductivity of 7713 S cm^{-1} through a large-scale wet-spinning. Wet spinning also realizes the expansion of carbon-based material into continuous conductive fibers with micro- and nanometric diameters. GO has attracted a lot of attention as a 2D sub-nano-thickness topology with unique synthetic scalability, superflexibility and chemical reactivity. Herein, Chang *et al.*[125] reported reversible fusion and fission of wet-spun GO fibers. Under the simulation of water and polar organic solvents, internal swelling led to the fusion and fission of GO fibers with recoverable properties and geometrical deformation, which showed the recyclability of multiple functional applications. Zheng *et al.*[126] successfully prepared hybrid microfibers composed of hyaluronic acid (HA) and MWCNTs, in which HA acted as a biosurfactant and ionic crosslinker for optimizing dispersion stability of MWCNTs. The obtained HA/MWCNT hybrid microfibers showed excellent electrical stability during cyclical mechanical deformation and twisted tests, which provided great application potential for MESDs. Cai *et al.*[127] reported ternary coaxial fibers composed of a ternary core (graphene/CNTs/PEDOT:PEE) and CMC (carboxyl methylcellulose) sheath. The CMC aqueous and the ternary dispersion were transferred to two injection syringes that were connected with the inner and outer channels of the spinneret and accordingly obtained ternary coaxial fibers by extruding spinning solutions into a coagulation bath. CNTs uniformly dispersed between graphene effectively prevented the restacking of graphene sheets, thereby, effectively increasing the contact area of ions. Consequently, the assembled SCs showed desirable area-specific capacitance of 396.7 mF cm^{-2} at 0.1 mA cm^{-2} and energy density of 13.8 μW h cm^{-2}. To sum up, spinning technology allows fibers controllable morphology and uniform distribution, which meet the requirement for devices with complex architectures.

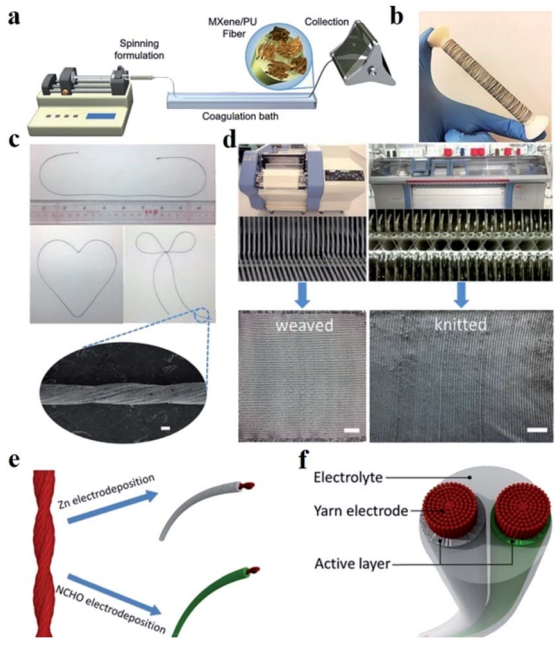

Fig. 7 (a) Schematic illustration of sinning process of the MXene/PU fiber. (b) Digital photograph of fabricated MXene/PU fiber. Reproduced with permission.[120] Copyright 2020, Wiley-VCH. (c) Flexibility demonstration and SEM image of the yarn. (d) Demonstration of weavability and knittability. (e) Schematics of yarns electrodeposited with Zn and NCHO and (f) solid-state yarn battery. Reproduced with permission.[121] Copyright 2017, American Chemical Society.

Thermal drawing sustains strong support for highly elastic and functional fibers used in wearable devices. There are two ways to produce functional fibers: the first one is to assemble all the materials together into a macroscopic prefab and draw within the prescribed architectures.[128] The second one is to draw a microstructured polymer or glass fiber as a template and to integrate functional materials within the prescribed positions. In 2004, the exploration of micro/nanofibers *via* thermal drawing technology was realized for the first time, in which Bayindir *et al.*[129] obtained a fiber by constructing an amorphous semiconductor core surrounded by metallic microwires and optically responsive polymers, which showed a size below 100 nm. Ren and co-workers[130] reported a micro-needle array electrode (MAE) assembled with glassy-state poly(lactic-*co*-glycolic acid) (PLGA) *via* the thermal drawing method. The pillar array contacted glassy-state PLGA film and moved upward at a certain speed, thus forming the MA tips. However, the integration of energy-harvesting systems based on thermal drawing technology still has many challenges such as battery life and energy storage.

3.3 Embedding electronic function in textile

In addition to the above ways to realize electrochemical characteristics, there are various conventional processes such as weaving, and knitting that play a significant role in the manufacture of textile-based electronic equipment. The woven yarn electrodes for wearable batteries necessitate both high electric conductivity and excellent mechanical strength. Here, Huang *et al.*[121] demonstrated a rechargeable yarn battery basis on woven yarns covered with zinc (as the anode) and nickel–cobalt

hydroxide nanosheets (as the cathode), which can expand conductive yarns into large-area conductive cloth integrated with various electronic devices. Zn and nickel–cobalt hydroxide (NCHO, as the cathode) were electrodeposited on yarns (Fig. 7e). Ascribed to intrinsic flexibility (Fig. 7c) and knittability (Fig. 7d), micron-sized stainless steel (316L) was used as conductive long yarns, and its superior conductivity in one-dimension endowed electron the transport capability for ultralong distance. Fig. 7f schematically shows a free-standing yarn battery. As a result, the fabricated yarn-based NiCo//Zn batteries delivered a high specific capacity of 5 mA h cm^{-3} and energy densities of 0.12 mW h cm^{-2} and 8 mW h cm^{-3}. Zeng and co-workers[131] utilized segmented polyurethane and silver-coated polyamide multifilament yarns as highly-elastic conducting knitted fabric to make up the electrodes of the nanogenerator. After twisting together with polyurethane multifilament yarn and a silver-coated polyamide multifilament yarn by yarn twister, the plain fabrics were knitted through a circular knitting machines equipped with a tension controller and thus obtained the fabric electrodes. Due to the induced localized strain gradients, the contact area of electrode increased and more flexoelectric effects are imposed. Loop structures of the knitted fabric electrodes provide reliable collection networks, which enhanced the durability and work efficiency of the nanogenerator for energy harvesting. Shi *et al.*[132] reported textile displays made of micrometer-scale electroluminescent units based on ZnS phosphor by weaving conductive weft and luminescent warp fibers acting as textile integration unit for various applications with outstanding breathability and washability.

In conclusion, whether endowing single fiber with unique electrical characteristics or loading electronic components on a large-area functional textile, existing efforts have provided a variety of customized solutions for fabrics from material preparation to processing manufacturing. The future direction of improvement can focus on mass production and the recyclability of raw materials.

4. Multiple applications

Textile-based wearable material, a very potential substrate in wearable MESDs, not only has the ability to power electronic devices but also has good mechanical reliability and excellent processability, which provides strong support in the manufacture of wearable MESDs with customizable shapes. This section mainly discusses the mechanical reliability of TMESDs, shape customizable manufacturing, self-charging function, self-healing function and sensing function.[133]

4.1 Mechanical reliability

Mechanical reliability (*e.g.*, mechanical strength, flexibility, stretchability, abrasion resistance, *etc.*) is a basic performance required by fabric-based MESDs in the field of wearable devices. Whether in the direction of 1D SCs or batteries, or 2D MESDs, the fabric-based devices exhibit excellent mechanical reliability.[134]

4.1.1 Mechanical reliability of yarn/fiber-shaped energy storage devices. Due to the excellent flexibility and ductility of 1D structures (such as carbon fiber, metal fiber, polymer fiber), when it is used as an active material loading or directly used as an electrode, the prepared energy storage device still has good mechanical reliability. Wang and co-workers[135] reported a sewable, wearable, and washable fiber zinc battery, which used polydopamine (PDA) loaded carbon fibers as a cathode, Zn wire as an anode, and PVA/zinc trifluoromethanesulfonate ($Zn(CF_3SO_3)_2$) as gel electrolyte. The battery showed excellent toughness and specific capacity (372.3 mA h g^{-1} at 50 mA g^{-1}). Even at a bending angle of 180°, the sewed power textile still showed excellent ultralong cycle stability. In addition, the linear battery can be sewn on other fabrics or woven into a wearable power fabric to power other devices (Fig. 8a). Washability is quite necessary for the environment in daily life activities such as raining and washing. The optimized PDA-based cathodes showed higher washing resistance than that of fiber electrodes prepared using the dip-coated method. Moreover, the PDA-coated fibers could maintain their shape well after hundreds of cleaning cycles. After the sewn power fabric was sealed with silica gel, it could be stirred and washed in water for 3 hours. Su *et al.*[138] adopted a strategy to convert the CNT forest grown on the silicon substrate into the CNT yarns, followed by the fabrication of core-sheath CNT/stainless steel using the flyer spinner. Finally, two core-sheath CNT/stainless steel was infiltrated by ion liquid (IL) gel electrolyte and twisted into

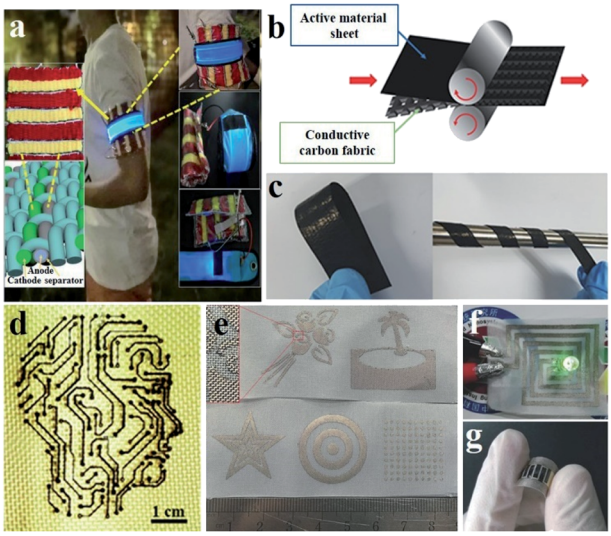

Fig. 8 (a) Batteries knitted into a sweater (the yellow arrow is pointing) and used as power sources lighting the LED bands. Reproduced with permission.[135] Copyright 2020, Wiley-VCH. (b) Schematic demonstration of the preparation process of the electrode. (c) Photograph of prepared flexible electrodes. Reproduced with permission.[136] Copyright 2018, Wiley-VCH. (d) Photograph of LIG patterned into a human side face shape. Reproduced with permission.[18] Copyright 2020, American Chemical Society. (e) Different conductive patterns drawing on two polyester fabrics. (f) The DC power source powered the green LED through the textile conductive circuit. (g) Photograph of fabricated textile MSC. Reproduced with permission.[137] Copyright 2016, Wiley-VCH.

a symmetrical SC. It showed a high voltage window of 2.7 V, a capacitance of 263.31 F cm^{-3} and a superior energy density of 6.67×10^{-2} W h cm^{-3}. Due to the mechanical properties of CNTs, the SC also exhibited amazing flexibility even when woven and knotted. Some active materials in textile device design may further strengthen the mechanical properties of the original substrates. It is reported that the tensile strength and Young's modulus of composite fibers are enhanced in comparison with pure polymer fibers. For example, the tensile strength increased from 334 MPa to 468 MPa when coated with 79 wt% of MXene on cotton yarn. In addition, the increase in the size of the MXene flakes is also proportional to the enhancement effect. Large flakes avoided defects and edges, thereby helping fiber's growth and its electrical conductivity and mechanical strength are effectively improved.[139] However, poor flexibility and non-stretchable active materials or conductive materials (such as bulk metal sheets) will reduce the flexibility and tensile performance of the MESDs.[140] Therefore, the actual requirements for energy supply and mechanical performance of MESDs can be met by selecting appropriate active materials, fabric substrates, electrolytes, electrode matching and structures, which is of great significance for wearable devices.

4.1.2 Mechanical reliability of sheet TMESDs. At present, the mechanical reliability of sheet TMESDs has also attracted great attention. Yuan *et al.*[141] loaded MXene onto N-doped carbon fiber textiles (NCFT) by repeated drying and coating processes and used PVA/H_2SO_4 gel as the electrolyte to form a solid ASC with oxidized carbon fiber textile. The ASC had an energy retention of 90% in more than 30 000 cycles at a current density of 5 mA cm^{-2}. Fixing MXene on the surface of the fiber substrate as a thin-film coating allowed ASC to be tailored into arbitrary shape in practice. In 2019, Zhang *et al.*[142] reported a facile self-degrading template method through a one-step chemical oxidation process. In this way, vertical polypyrrole (PPy) nanotube arrays and carbon nano-onions (CNOs) were loaded on the spandex fabric to fabricate electrodes for SCs. The electrodes and PVA/H_3PO_4 gel electrolyte were assembled into a sandwiched SC. The SC showed a capacitance of 64 F g^{-1} and capacitance retention of 99% after 500 stretching cycles at 50% strain. Smart conductive textiles are regarded as current collectors for LIBs due to their native networks. With the continuous update in smartwatches, higher requirements are placed on the flexibility and capacity of the LIB. Lee *et al.*[136] further enhanced electrode conductivity and flexibility of LIBs by nanosizing lithium titanate oxide (LTO) and lithium iron phosphate (LFP), and hybridizing them with a flexible 2D graphene template. In this work, $LiFePO_4$/rGO cathode and LTO/rGO anode were obtained by a hydrothermal method and annealing, and the carbon fiber fabric was rolled press together through a polytetrafluoroethylene (PTFE, linking agent) to obtain LTO/LFP full cell (Fig. 8b). The internal 3D fiber network of the fabric is particularly advantageous for interfacial contact between the active material and current collector, therefore ensuring reliable mechanical performance during daily wear. The high level of flexibility can be clearly shown in the photograph shown in Fig. 8c. The as-prepared LIB showed a large capacity of 1.2 mA h cm^{-2}, and it could still maintain 99.5% of the initial open-circuit voltage (OCV) after 1000 bending cycles at a bending radius of 10 mm.

Other reported materials such as the poly(3,4-ethylenedioxythiophene) polystyrene sulfonate (PEDOT:PSS),[84] CNF,[96] and AgNW composite fiber,[64] also showed great potential in wearable fabric energy storage. These materials possess high stability, excellent mechanical properties and high electrical conductivity.[123,143]

TMESDs have high mechanical stability and cycling stability as reported in many studies. Most studies only focused on the performance of unidirectional stretching and bending, while there were relatively few reports on large-angle torsion and multi-directional stretching. In addition, the researches on the thermal stability and abrasion resistance of TMESDs at extreme temperatures are rare, which also inhibit the practical application of TMESDs.[136]

4.2 Shape customizable manufacturing

Due to their excellent mechanical reliability, textile-based devices can be designed in a fashionable way with proper wearable technology. There are generally two ways to make TMESDs of different shapes: (1) by fabricating a 1D energy storage device such as optical fiber or yarn, which can be made into MSCs and MBs of different shapes through weaving, sewing, and cutting the 1D MESDs; (2) through some patterning processes such as photolithography, laser printing, screen printing and other methods to prepare electrodes on the 2D textile, which can be further combined with electrodeposition, chemical vapor deposition (CVD), physical vapor deposition (PVD) and other technologies to load the active materials on the patterned electrodes; (3) through subsequent operations such as filling electrolyte and encapsulating, which endow the TMESDs with different patterns.[19,144]

4.2.1 Wearable customized for yarn/fiber shaped textile-based MESDs. The ingenious design and incorporation of brick materials such as polymers and nanomaterials on textiles offer customizable functions for wearable devices. However, the active coating on the fabric will inevitably pose negative effects on flexibility and breathability. Herein, Guan *et al.*[145] designed a 3D conformal porous microstructure through a breath figure technique. The obtained porous microstructured textiles not only have an adjustable shape with retaining of the inherent properties of the cotton but also have new functions like triboelectric function and moisture permeability, demonstrating great potential in the applications of self-power pressure sensors with all-textile structures. Attributed to the inherent excellent mechanical reliability and flexibility of the yarn-shaped or fiber-shaped fabric energy storage devices, it could withstand large mechanical deformations. Even if it is treated by weaving, sewing, cutting, *etc.*, it will not have an excessive impact on the performance of the textile-based energy storage device. Therefore, the fiber/yarn electrode can be processed into various patterns and used in wearable devices. Zheng *et al.*[146] wrapped a Ni layer on cotton thread and deposited rGO to obtain the electrode structure of ErGO/Ni-cotton,

and embroidered stainless steel yarns on the edge of the electrode as conductive contacts. In a similar way to interdigital SCs and sandwich SCs, the electrode can be combined into various patterns, and they can be sewn and fixed on other fabrics by using non-conductive yarns. After coating with a waterproof layer, the prepared wearable SC has good mechanical properties and washability. In order to expand the application of wearable MSCs and wearable MBs, the integration of TMESDs with other functional units has attracted great attention. Mai *et al.*[147] coated TiN nanowires (NWs), a kind of pseudocapacitance materials and carbon shell on the Ti wire through a hydrothermal method to prepare TiN/Ti electrode. After that, the two electrodes were put into a plastic tube and PVA/KOH gel electrolyte was injected to assemble a fiber-shaped SC. The group also grew ZnO nanowires on Mn-coated Ti wire and coated dye N719 and a hole-transfer layer (CuI) to obtain a photoanode. Then, the Cu-coated polymer wire and cotton yarn were used to connect and weave multiple photoanodes together and integrate with TiN/Ti fiber-shaped MSCs. Since both TiN/Ti electrodes and photoanodes can be woven, cut, and sewn, the integrated energy storage and energy conversion device can be customized into a stylish self-powered wearable energy storage device.

4.2.2 Wearable customized of MESDs based on stacked textile. As a convenient and facile method for fabricating 2D patterns, laser printing has received a lot of attention in the manufacture of customized wearable TMESDs. In 2012, Kady *et al.*[67] reported a method to fabricate rGO-coated on commercial optical discs with laser irradiation. In 2014, Tour *et al.*[148] used lasers to write on polyacrylamide (PI), which could directly convert the area irradiated by the laser into patterned graphene electrodes.

Laser writing technology provides a desirable way for the integration of electronic devices into traditional clothing. Wang and co-workers[75] used laser writing to prepare patterned graphene/Kevlar textile and then fabricated a Co_3O_4–graphene/Kevlar textile as a cathode for Zn–air battery. Furthermore, researchers fabricated self-powered protective clothing (Fig. 8d) with graphene/Kevlar textile-based Zn–air battery, the system could continuously supply power for 12 h at a current density of 0.05 mA cm^{-2}. Gu *et al.*[149] fabricated graphene SCs in 3 minutes on Spandex Nylon Lycra Matte fabrics coated with waterproof polydimethylsiloxane (PDMS) elastomer on one side and GO coated on the other side. The obtained SC possessed an areal capacitance of 49 mF cm^{-2}, an energy density of 6.73 mW h cm^{-2}, a power density of 2.5 mW cm^{-2}, and the SC could also be directly integrated with washable silicon solar cell to achieve a self-powered purpose. In 2016, Wang and co-workers[137] showed a method of laser-scribing masking that different shapes of masks were utilized in the preparation of laser-scribing electrodes, as schematically shown in Fig. 8e. Afterward, through the subsequent electroless deposition and hydrothermal reactions with GO aqueous solutions, Ni and rGO can be respectively coated on the electrodes, which can be well integrated into clothing with the flexibility (Fig. 8f and g). In another work, Wang *et al.*[19] used a resist dyeing method with conductive dyes in textile micro-AZB. The resist substances such as wax, rice paste, stencils, and strings can prevent unwanted areas from dyeing on the textile while other areas can absorb conductive dyes. In this way, different patterns of electrode shapes can be made on the fabric substrate. After that, Zn nanosheets/NiCo BOH pattern was deposited by electroplating and the gel electrolyte was applied to make a solid Zn-ion battery, which could be integrated into clothing to make a fashionable wearable device.

With the development of wearable fabric MESDs, it is not necessary to only meet the performance requirements of the actual use of fabric-based energy storage, but also to meet the public's aesthetic requirements for wearable electronic devices and wearable smart clothes, which is also a very important factor in the productization of wearable devices.

4.3 Self-charging function

To satisfy the growing power demand and eliminate charging frequency, there are wearable integrated energy collectors with self-sustainable system, such as solar cells, friction generators, enzymes, or microbial fuel cells, to make them self-sustainable.[19] However, the operation of these systems depends on a single input source and the harsh working conditions to make the effect of their implementation not ideal.

The fiber material meets the demands of lightness and wear resistance. The additional function of self-charging, as a sustainable way of using energy, is expected with great promise in MESDs. To develop a practical strategy to remove multiple types of energies from the environment at the same time, a concept of hybrid energy harvester is proposed. However, mixing multiple collectors that are not cooperative in the real scene mostly leads to the introduction of additional restrictions rather than compensation for the existing limited situation.[150] Therefore, the research on a better hybrid system is imminent.

For example, Wang[151] proposed and demonstrated the concept of wearable electronic textile microgrid system powered by complementary and collaborative energy collectors and corresponding energy storage modules. Different from the early hybrid wearable system, the current e-textile microgrid only relies on human activities to work together. It used sweat-based biofuel cells (BFCs) and friction generators (TEG) to collect biochemical energy and biochemical energy and adjust the collected energy through super capacitors to realize self-power supply.[150] In addition, others proposed a prototype of a new fabric hybrid self-charging power system,[152] which was useful not only to collect solar energy from ambient light but also to collect mechanical energy from human movement. For fibrous dye-sensitized solar cell (f-DSSCs) and fibrous tendons (f-tendons, for mechanical energy), it is easy to convert the two kinds of harvested energy into electrical energy, which can be further stored as chemical energy in fibrous SCs (F-SCs). The hybrid self-charging textiles not only achieve reasonable energy conversion and storage capacity, but also are cheap and easy to manufacture. In addition, since each device has an all-fiber shape, the proposed hybrid self-charging textile system can be

easily woven into electronic textiles to manufacture intelligent garments for operating wearable electronic devices.

4.4 Sensing function

The sensing function is to sense the external pressure signal and convert it into an electrical signal according to a certain working principle. Current research focus on textile-based sensors includes temperature sensors,[153] pressure sensors,[154] electromagnetic induced sensors[155] and strain gauge sensors.[156] Among them, pressure sensors are widely used in comfortable and intelligent wearable electronic devices. Generally, there are four sensing mechanisms of flexible wearable pressure sensors: piezoresistive, capacitive, piezoelectric and triboelectric.[157] Piezoresistive pressure sensor generally adopts a sandwich structure, two flexible electrodes and a piezoresistive layer sandwiched in the middle. It can also be simplified as a two-layer structure with a cross electrode at the bottom and a piezoresistive layer at the top. When the piezoresistive flexible pressure sensor is stimulated by external pressure, the middle piezoresistive material will deform and change the resistance of the device.[158] By measuring the change of stress-induced resistance, the change of external pressure can be inferred. An easy approach to manufacture textile pressure sensor is proposed by Pizarro *et al.*[159] It was made using a low-cost conventional antistatic sheet and conductive motor fabric and had a typical sandwich structure. When the proposed sensor was installed on the glove, the impulse response was accurately distinguished and translated into the pressure variations, thus showing application potential in medical telemonitoring and health assessment. The advantages of resistive sensors are simple structure, high detection sensitivity, short response time, large detection range, and low power consumption. In order to improve the sensing performance of the piezoresistive sensor, it is necessary to increase the number of contact points and the accumulated contact interface area under pressure, such as pyramid structure, concave–convex structure, or tooth structure. Herein, Tan *et al.*[154] reported a fully-textile sensor consisting of rGO–cotton fabric electrodes and Ag fabric electrodes. After integrating with the proposed sensor, the obtained monitoring insole provided a stable signal and finely captured time–pressure data under different contact pressures, which held application promises in sports monitoring and e-skins.

Another method of signal conduction is to use the capacitance change of dielectric materials between conductive electrodes. Usually, the typical structure of a capacitive sensor is a sandwich structure composed of an elastic medium layer sandwiched between two parallel plate electrodes. Two flexible conductive fabrics are used as electrode plates, separated from flexible dielectric spacers (such as foams, fabric spacers and soft polymers). To date, Chen and co-workers[162] developed a topographical modification for the improved conductivity and durability of the wearable capacitive sensors. The device realized simultaneous detection of the change of distance and angle, therefore recording dynamic information such as speaking, blinking, head movement and joint movement in real-time. Capacitive pressure sensors usually have good linearity and low-pressure detection limit, but compared with the piezoresistive pressure sensor, its sensitivity is relatively low.[163] Therefore, to effectively improve the sensitivity of the capacitive sensor, large deformation of the electrode and dielectric layer must be realized even under low external stress, which can be improved by using an elastic electrode or microarray structure. For example, Vu *et al.*[164] added Ag ink to the textile sensor, which guaranteed conductivity and flexibility in actual applications. Keum *et al.*[165] embedded Ag-plated conductive fiber electrodes in fabrics, thus obtained capacitive pressure sensors with high sensitivity and high operation stability. Owing to the matrix-type array structure, multi-point and different positions are detected precisely.

Piezoelectricity is the ability of a material to generate an internal electric field under mechanical stress or strain. The wearable fabric pressure sensor with piezoelectric characteristics can convert the external pressure into electric energy to detect the movement of the human body based on the force applied on the sensor. When piezoelectric materials are subjected to mechanical pressure and generate positive and negative charges, polarization occurs. By quantifying the voltage or current on the device, the external pressure stimulation can be evaluated.[166] To improve the interfacial adhesion between fibers, Su *et al.*[167] dispersed polydopamine (PDA) into the electrospun nanofibers. By creatively mimicking the muscle fibers, the fabricated piezoelectric textile showed high biocompatibility, thus paving a cost-effective way to realize wearable personalized healthcare such as pulse wave measurement and active voice recognition. It is suitable for the piezoelectric sensor to provide the dynamic measurement of acoustic vibration, slip, and other pressures due to its high sensitivity and fast response. Piezoelectric sensors do not need an external energy supply, so it is an ideal choice to develop low-power or even self-powered sensing devices and energy acquisition devices.[168]

The triboelectric effect, or triboelectrification, is a well-known phenomenon. Triboelectrification is a very common phenomenon.[169] By using this electrostatic induction phenomenon, mechanical motion can be transformed into the generation of surface charge, thus driving the current to flow through the external circuit, so that the mechanical energy can be transformed into usable electric energy. Zhu *et al.*[160] reported a triboelectric sensor without any power supply based on thin-film material as shown in Fig. 9a. By charging the contact and generating a voltage signal, the self-powered triboelectric sensor is promising to solve the problem of power consumption of the sensor unit, and realize an ultrahigh level of pressure sensitivity and touch sensitivity (Fig. 9b). In the coming era of intelligence, wearable electronic devices will show great application prospects in the energy collection of biological movement and multi-functional self-powered sensors.

4.5 Self-healing function

Similar to the self-recovery of human skin, self-healing refers to the self-repair of electrochemical properties and structural integrity after suffering severe external mechanical damage.[170] As far as flexible and scalable energy storage devices are

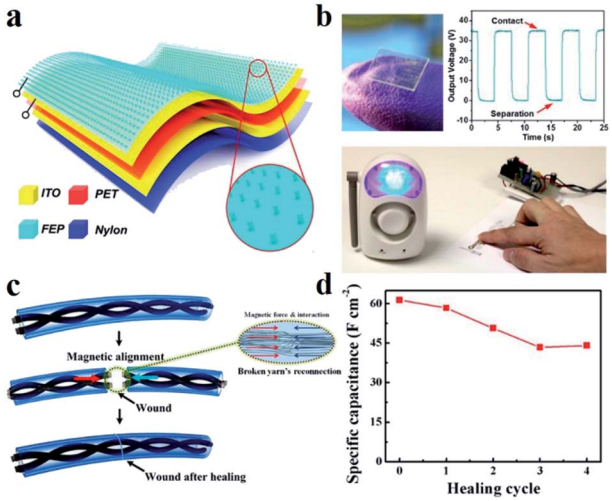

Fig. 9 (a) Schematic illustration of the self-powered triboelectric sensor (TES). Inset: Enlarged view of polymer nanowire on the top surface. (b) Photograph of an as-fabricated triboelectric sensor (left), the output voltage of triboelectric sensor at a contact pressure of 0.03 kPa when sensing a metal object (right), and tap TES to trigger the wireless alarm system (below). Reproduced with permission.[160] Copyright 2014, American Chemical Society. (c) Schematic illustration of the self-healing process of SC. (d) The specific capacitance of the original device and after cyclic self-healing. Reproduced with permission.[161] Copyright 2015, American Chemical Society.

concerned, the inevitable structural fracture and mechanical damage caused by repeated stretching and bending can lead to electrochemical performance degradation and even safety problems.[171] Especially when flexible/scalable MESDs are integrated with implanted bioelectronics, the replacement of any damaged battery or SC is complicated and unsafe. Therefore, the life of the power supply will determine the service time. According to the pioneering classification,[172] the mechanism of artificial self-healing can be divided into three categories: (1) according to capsule based self-healing, self-healing mechanism is initiated by releasing healing agent in the injured area, which is a single and unrepeatable healing process;[173] (2) according to blood vessel based self-healing, healing agents are released from the interconnected hollow channels to achieve repeated geofunctional self-healing process;[174] and (3) intrinsic self-healing is achieved by molecular diffusion and entanglement or by inherent reversible chemical bonds, such as covalent or noncovalent bonds.[135]

4.5.1 Capsule-based self-healing mechanism. A capsule-based self-healing mechanism was initially developed by White *et al.*[173] In this mechanism, functional healing agents such as monomers and catalysts (initiators) were encapsulated in microcapsules in a polymer matrix. As long as the damage triggers the breaking and release of the healing agent, the self-healing process was initiated by the polymerization between the healing agent and the catalyst, followed by the physical filling of cracks, reduction of mechanical structure and chemical properties without any external stimulation. Capsule-based self-healing is an independent recovery process without any external stimulation. It can achieve the purpose of self-healing, while local polymerization occurs at the fracture interface. However, in terms of capsule-based self-healing mechanism, the local healing agent will be consumed after the release to fill the crack area. This shows that a self-healing capsule can only promote a single healing event, so it is an irreversible and unrepeatable self-healing process.[175]

4.5.2 Vascular-based self-healing mechanism. In order to eliminate the shortcomings of capsule-based self-healing mechanisms, blood vessel-based self-healing expands the healing agent to capillaries or hollow channels, which become a network connected with each other to achieve a repeatable self-healing process. White *et al.*[174] introduced a 3D microvascular network, which was not a discrete capsule filling-healing agent. Microvascular structures can also act as reservoirs for the storage of healing agents, based on their multiple connection points and highly connected channels. It can complement the networks connected to each other and can heal repeatedly, even in multiple damage events. Therefore, this kind of vascular structure can achieve repeatable self-healing for local injury according to its own continuous self-healing agent supply. Self-healing hydrogels are widely employed as the potential mainstay of electronic skin and soft skins due to their functional tunability. Although MXene-based hydrogels excel in conductivity, there exists room for improvement in stretchability and functional tunability. Ge *et al.*[176] used MXene as a dynamic cross-linker lead and explored its excellent adhesion and self-healing abilities through fast gelation with different polymeric hydrogels. The introduction of MXene hydrogels obviously increased the mechanical robustness and stretchability of various hydrogels, showing the potential application in soft robots, 3D-printed electronics and wearable devices with self-healing power. The self-healing based on blood vessel achieves the repeated healings of multiple damaged electrodes, while the complexity of microvascular structure in electrode materials hinders its universal application in healing electrodes. Many physicochemical properties of vascular structure or capsule, such as wettability, viscosity, chemical reactivity and even interface compatibility, need to be improved, so as to achieve high efficiency and good circulation self-healing performance.[149]

4.5.3 Intrinsic reversible self-healing mechanism. An intrinsic self-healing process is achieved through reversible molecular diffusion, entanglement, covalent reaction, hydrogen bonding or ionomer/supramolecular rearrangement.[172] Generally speaking, the mechanical damage of the polymer network will lead to chain rupture and/or slippage, and then reactive groups will be generated at the damaged interface. Internal self-healing materials do not need the participation of healing agents but do need external stimulation, such as high temperature,[177] ultraviolet radiation,[178] and pH,[179] to start the self-healing reaction. Huang *et al.*[161] reported a self-healable yarn-based SC by wrapping magnetic electrodes around a self-healing polymer shell as shown in Fig. 9c. After four fracture/healing cycles, the specific capacitance can be restored to 71.8% (Fig. 9d). Generally, the self-healing mechanism can be divided into three categories: intermolecular diffusion, covalent bond and noncovalent bond.[180] Once the material is destroyed,

it immediately activates the healing process to repair the cracks, including the steps of molecular rearrangement and surface approaching, interphase wetting, mutual diffusion, and molecular chain re-entanglement.[84]

Covalent bond-based self-healing processes usually rely on reversible covalent reactions, including the transformation from discrete monomers to interconnected polymers by external stimuli such as light or heat. Because of the strong bonding from the covalent bond, the self-healing process based on covalent bond endows healing materials with higher mechanical strength.

Noncovalent bond-based self-healing is another promising mechanism. Even without external stimulation or heating, hydrogen bonds, ionomers and metal bonds can be used to recover damage.[181]

The integration of self-healing abilities can effectively alleviate the degradation of mechanical strength, and enhance the electrochemical performance and service life by repairing cracks, fractures and delamination during repeated deformation. To some extent, self-healing flexible/scalable MESDs provide exact solutions to restore mechanical and electrochemical performance, and achieve the reliability and durability required for practical applications.

5. Conclusion and perspective

The growing demand for miniaturized flexible devices will lead to the rapid development of TMESDs and derive a variety of applications. In this review, the constructing methods of TMESDs, the role of fabrics in flexible MESDs and the applications that meet the actual scenarios are elaborated and summarized, so as to systematically describe the development of TMESDs. Following the introduction to device design, several typical microfabrication techniques are discussed in details and compatibility with fabric still needs much attention. We elaborated the construction of thin-film MESDs and fiber-shaped MESDs from the perspective of the electrode material. Commercial fabrics have better control of cost while making higher requirements of other functional additives and active agents. Given interdigital MESDs, we believe the compatibility between microelectrode materials and the process of precise micro–nano fabrication will pave the way for higher energy and power densities. Furthermore, we summarized the processing strategies of functionalized fibres based on their different dimensions. By preparing a single conductive unit or integrating electronic function into large-area textiles, functionalized improvements are achieved, providing the ordinary fabric more opportunities and a more intelligent life to match people's desires. Regarding practical applications, realistic requirements such as energy storage, mechanical reliability, customizable shapes, sensing, and self-healing are put forward. In the future, electronic integration on comfortable clothing will probably appear as a display screen or a real-time monitor. And a rapid increase in innovative research results and publications is emerging. Despite great achievements, there are still some critical challenges. These improvements mainly concentrate on rational designs, new microconstruction techniques, and innovative electrode materials. For security purposes, it is necessary to consider replacing the toxic element in electrolyte with degraded polymer. From the point of microfabrication technique, it is a challenge for miniaturization processes to coexist with material preparation, such as obtaining high-resolution patterns without destroying the growth of active materials. When meeting the demand for power sources, some actual requirements such as washability, less occupancy of space, lightweight also make sense. Besides, there are more cooperative ways between textile and nanomaterials to be explored. The new smart textiles will be presented in future studies.

Author contributions

Yixue Duan, Gongchuan You, Liang He and Bin Xu discussed the outline and wrote the manuscript. Kaien Sun, Zhe Zhu discussed and summarized the related progress on "Device design". Xiaoqiao Liao and Linfeng Lv discussed and summarized the related progress on "Technique fundamental". Yixue Duan and Hui Tang discussed and summarized the related progress on "Multiple applications". All the authors participated in the discussion, writing and revision of this review.

Conflicts of interest

There are no conflicts to declare.

Acknowledgements

This work was supported by the Fundamental Research Funds for the Central Universities (20822041E4045) and the Fund of Science and Technology on Reactor Fuel and Materials Laboratory (STRFML-2020-24).

References

1 C. Lethien, J. Le Bideau and T. Brousse, *Energy Environ. Sci.*, 2019, **12**, 96–115.
2 S. Park, Z. Khan, T. J. Shin, Y. Kim and H. Ko, *J. Mater. Chem. A*, 2019, **7**, 1564–1573.
3 W. Yang, L. He, X. Tian, M. Yan, H. Yuan, X. Liao, J. Meng, Z. Hao and L. Mai, *Small*, 2017, **13**, 1700639.
4 X. Ma, S. Feng, H. Liang, M. Yan, X. Tian, Y. Li, C. Tang, X. Hong and L. Mai, *Nanoscale*, 2017, **9**, 11765–11772.
5 L. B. Hu and Y. Cui, *Energy Environ. Sci.*, 2012, **5**, 6423–6435.
6 H. Bing, Q. Zhang, L. Li, J. Sun, M. Ping, Z. Zhou, Q. Li, J. Guo, L. Xie and C. Li, *J. Mater. Chem. A*, 2018, **6**, 14594–14601.
7 L. L. Wang, K. Jiang and G. Z. Shen, *Adv. Mater. Technol.*, 2021, **6**, 2100107.
8 X. Li, R. Liu, C. Xu, Y. Bai, X. Zhou, Y. Wang and G. Yuan, *Adv. Funct. Mater.*, 2018, **28**, 1800064.
9 Y. Yang, Q. Huang, L. Niu, D. Wang, C. Yan, Y. She and Z. Zheng, *Adv. Mater.*, 2017, **29**, 1606679.
10 X. Pu, L. X. Li, M. M. Liu, C. Y. Jiang, C. H. Du, Z. F. Zhao, W. G. Hu and Z. L. Wang, *Adv. Mater.*, 2016, **28**, 98–105.

11 H. Sun, S. Xie, Y. Li, Y. Jiang, X. Sun, B. Wang and H. Peng, *Adv. Mater.*, 2016, **28**, 8431–8438.
12 L. L. Liu, Z. Q. Niu, L. Zhang, W. Y. Zhou, X. D. Chen and S. S. Xie, *Adv. Mater.*, 2014, **26**, 4855–4862.
13 Z. Wen, M. H. Yeh, H. Y. Guo, J. Wang, Y. L. Zi, W. D. Xu, J. N. Deng, L. Zhu, X. Wang, C. G. Hu, L. P. Zhu, X. H. Sun and Z. L. Wang, *Sci. Adv.*, 2016, **2**, e1600097.
14 J. Lim, D. S. Choi, G. Y. Lee, H. J. Lee, S. P. Sasikala, K. E. Lee, S. H. Kang and S. O. Kim, *ACS Appl. Mater. Interfaces*, 2017, **9**, 41363–41370.
15 S. Kwon, T. S. Lee, H. J. Choi, J. Y. Ahn, H. J. Lim, G. H. Kim, K. B. Choi and J. J. Lee, *J. Power Sources*, 2021, **481**, 228939.
16 Y. X. Chen, Z. R. Deng, R. Ouyang, R. H. Zheng, Z. Q. Jiang, H. Bai and H. Xue, *Nano Energy*, 2021, **84**, 105866.
17 Z. Dai, F. F. Yan, M. Qin and X. Yan, *E-Polymers*, 2020, **20**, 600–605.
18 H. M. Wang, H. M. Wang, Y. L. Wang, X. Y. Su, C. Y. Wang, M. C. Zhang, M. Q. Jian, K. L. Xia, X. P. Liang, H. J. Lu, S. Li and Y. Y. Zhang, *ACS Nano*, 2020, **14**, 3219–3226.
19 M. M. Liu, X. Pu, Z. F. Cong, Z. X. Liu, T. Liu, Y. H. Chen, J. Q. Fu, W. G. Hu and Z. L. Wang, *ACS Appl. Mater. Interfaces*, 2019, **11**, 5095–5106.
20 J. Tan, Y. L. Han, L. He, Y. X. Dong, X. Xu, D. N. Liu, H. W. Yan, Q. Yu, C. Y. Huang and L. Q. Mai, *J. Mater. Chem. A*, 2017, **5**, 23620–23627.
21 M. Lou, I. Abdalla, M. Zhu, J. Yu, Z. Li and B. Ding, *ACS Appl. Mater. Interfaces*, 2019, **12**, 1597–1605.
22 N. A. Kyerematen, T. Brousse and D. Pech, *Nat. Nanotechnol.*, 2016, **12**, 7–15.
23 D. S. Yu, Q. H. Qian, L. Wei, W. C. Jiang, K. L. Goh, J. Wei, J. Zhang and Y. Chen, *Chem. Soc. Rev.*, 2015, **44**, 647–662.
24 C. García Núñez, L. Manjakkal and R. Dahiya, *npj Flexible Electron.*, 2019, **3**, 1–24.
25 S. Y. Chang, H. Kim, T. Lim, H. J. Kim, S. Cho, R. C. Kang, Y. S. Kim, K. S. Min, J. Yoo and S. Ju, *J. Mater. Chem. C*, 2017, **5**, 12825–12832.
26 Z. Tao, G. Zhang, F. Zhou, S. Zhang and D. Chao, *Small*, 2018, **14**, 1802320.
27 Y. Wang, X. Hong, Y. Guo, Y. Zhao and L. Mai, *Small*, 2020, **16**, 2000293.
28 W. Kai, Q. Meng, Y. Zhang, Z. Wei and M. Miao, *Adv. Mater.*, 2013, **25**, 1494–1498.
29 X. Peng, L. L. Peng, C. Z. Wu and Y. Xie, *Chem. Soc. Rev.*, 2014, **43**, 3303–3323.
30 Z. N. Tian, Z. T. Sun, Y. Y. Shao, L. Gao, R. Huang, Y. L. Shao, R. B. Kaner and J. Y. Sun, *Energy Environ. Sci.*, 2021, **14**, 1602–1611.
31 Z. Zhu, R. Kan, S. Hu, L. He, X. Hong, H. Tang and W. Luo, *Small*, 2020, **16**, 2003251.
32 J. Shi, S. Liu, L. Zhang, B. Yang, L. Shu, Y. Yang, M. Ren, Y. Wang, J. Chen and W. Chen, *Adv. Mater.*, 2020, **32**, 1901958.
33 H. Xia, Q. Y. Xia, B. H. Lin, J. W. Zhu, J. K. Seo and Y. S. Meng, *Nano Energy*, 2016, **22**, 475–482.
34 U. Gulzar, S. Goriparti, E. Miele, T. Li, G. Maidecchi, A. Toma, F. De Angelis, C. Capiglia and R. P. Zaccaria, *J. Mater. Chem. A*, 2016, **4**, 16771–16800.
35 X. Hong, X. Ma, L. He, Y. Dai, X. Pan, J. Zhu, W. Luo, Y. Su and L. Mai, *Small*, 2021, **17**, 2007791.
36 K. Brousse, S. Pinaud, S. Nguyen, P. Fazzini and P. Simon, *Adv. Energy Mater.*, 2019, **10**, 1903136.
37 J. Y. Shieh, S. Y. Tsai, B. Y. Li and H. H. Yu, *Mater. Chem. Phys.*, 2017, **195**, 114–122.
38 S. Xia, J. Ni, S. V. Savilov and L. Liang, *Nano Energy*, 2018, **45**, 407–412.
39 W. Chang, Y. Cao, Z. Luo, G. Li and D. Fang, *Chem. Eng. J.*, 2017, **307**, 382–388.
40 L. L. Liu, Z. Ji, S. Y. Zhao, Q. Y. Niu and S. Q. Hu, *J. Mater. Chem. A*, 2021, **9**, 6172–6179.
41 S. W. Song, K. C. Lee and H. Y. Park, *J. Power Sources*, 2016, **328**, 311–317.
42 B. Yao, J. Zhang, T. Kou, Y. Song, T. Liu and Y. Li, *Adv. Sci.*, 2017, **4**, 1700107.
43 M. Nasreldin, S. de Mulatier, R. Delattre, M. Ramuz and T. Djenizian, *Adv. Mater. Technol.*, 2020, **5**, 2000412.
44 S. A. Peng, B. Mqa, A. Ml, B. Wm, A. Gc and A. Yt, *Nano Energy*, 2019, **55**, 506–515.
45 N. Karim, S. Afroj, A. Malandraki, S. Butterworth, C. Beach, M. Rigout, K. S. Novoselov, A. J. Casson and S. G. Yeates, *J. Mater. Chem. C*, 2017, **5**, 11640–11648.
46 J. Yun, Y. Lim, H. Lee, G. Lee, H. Park, S. Y. Hong, S. W. Jin, Y. H. Lee, S. S. Lee and J. S. Ha, *Adv. Funct. Mater.*, 2017, **27**, 1700135.
47 W. Yang, Y. Zhu, Z. Jia, L. He, L. Xu, J. Meng, M. Tahir, Z. Zhou, X. Wang and L. Mai, *Adv. Energy Mater.*, 2020, **10**, 2001873.
48 Y. Zeng, Y. Meng, Z. Lai, X. Zhang, M. Yu, P. Fang, M. Wu, Y. Tong and X. Lu, *Adv. Mater.*, 2017, **29**, 1702698.
49 Z. Wang, J. Cheng, Q. Guan, H. Huang, Y. Li, J. Zhou, W. Ni, B. Wang, S. He and H. Peng, *Nano Energy*, 2018, **45**, 210–219.
50 G. Xiong, P. He, B. Huang, T. Chen, Z. Bo and T. S. Fisher, *Nano Energy*, 2017, **38**, 127–136.
51 G. Qu, J. Cheng, X. Li, D. Yuan, P. Chen, X. Chen, B. Wang and H. Peng, *Adv. Mater.*, 2016, **28**, 3646–3652.
52 J. Yu, W. Lu, J. P. Smith, K. S. Booksh, L. Meng, Y. Huang, Q. Li, J. H. Byun, Y. Oh and Y. Yan, *Adv. Energy Mater.*, 2017, **7**, 1600976.
53 H. Lu, J. Chen and Q. Tian, *J. Colloid Interface Sci.*, 2017, **513**, 342.
54 W. A. Haider, M. Tahir, L. He, H. Mirza, R. Zhu, Y. Han and L. Mai, *ACS Cent. Sci.*, 2020, **6**, 1901–1915.
55 J. Yan, Y. Ma, C. Zhang, X. Li and S. Luo, *RSC Adv.*, 2018, **8**, 39742–39748.
56 S. Yehezkel, M. Auinat, N. Sezin, D. Starosvetsky and Y. Ein-Eli, *J. Power Sources*, 2016, **312**, 109–115.
57 T. F. Qin, S. L. Peng, J. X. Hao, Y. X. Wen, Z. L. Wang, X. F. Wang, D. Y. He, J. C. Zhang, J. Hou and G. Z. Cao, *Adv. Energy Mater.*, 2017, **7**, 1700409.
58 J. Zhu, S. Zhao, X. Wu, Y. Wang, L. Yu and C. Nan, *Electrochim. Acta*, 2018, **282**, 784–791.
59 Z. A. Peng, W. A. Ni, A. My, B. Hr and A. Wh, *Chem. Eng. J.*, 2020, **380**, 122488.

60 M. Hu, T. Hu, R. Cheng, J. Yang, C. Cui, C. Zhang and X. Wang, *J. Energy Chem.*, 2017, **27**, 161–166.
61 L. Bao and X. Li, *Adv. Mater.*, 2012, **24**, 3246–3252.
62 Z. H. Yang and H. Q. Wu, *Solid State Ionics*, 2001, **143**, 173–180.
63 L. Shen, D. Bing, N. Ping, G. Cao and X. Zhang, *Adv. Energy Mater.*, 2013, **3**, 1484–1489.
64 L. Zhang, D. Liu, Z. S. Wu and W. Lei, *Energy Storage Mater.*, 2020, **32**, 402–417.
65 Q. Jiang, N. Kurra, C. Xia and H. N. Alshareef, *Adv. Energy Mater.*, 2017, **7**, 1601257.
66 S. V. Morozov, K. S. Novoselov, M. I. Katsnelson, F. Schedin, D. C. Elias, J. A. Jaszczak and A. K. Geim, *Phys. Rev. Lett.*, 2007, **100**, 016602.
67 M. F. El-Kady and R. B. Kaner, *Nat. Commun.*, 2013, **4**, 1475.
68 L. Zhang, D. Dearmond, N. T. Alvarez, R. Malik, N. Oslin, C. Mcconnell, P. K. Ad Usei, Y. Y. Hsieh and V. Shanov, *Small*, 2017, **13**, 1603114.
69 J. L. Ye, H. B. Tan, S. L. Wu, K. Ni, F. Pan, J. Liu, Z. C. Tao, Y. Qu, H. X. Ji, P. Simon and Y. W. Zhu, *Adv. Mater.*, 2018, **30**, e1801384.
70 L. Liu, D. Ye, Y. Yu, L. Liu and Y. Wu, *Carbon*, 2017, **111**, 121–127.
71 L. Liu, H. Y. Li, Y. Yu, L. Liu and Y. Wu, *Nanotechnology*, 2018, **29**, 055401.
72 Z. S. Wu, K. Parvez, A. Winter, H. Vieker, X. Liu, S. Han, A. Turchanin, X. Feng and K. Müllen, *Adv. Mater.*, 2014, **26**, 4552–4558.
73 W. W. Liu, C. X. Lu, X. L. Wang, R. Y. Tay and B. K. Tay, *ACS Nano*, 2015, **9**, 1528–1542.
74 C. W. Kan and C. W. M. Yuen, *Surf. Coat. Technol.*, 2013, **228**, S607–S610.
75 L. Li, V. Breedveld and D. W. Hess, *ACS Appl. Mater. Interfaces*, 2013, **5**, 5381–5386.
76 M. Q. Xue, Z. Xie, L. S. Zhang, X. L. Ma, X. L. Wu, Y. G. Guo, W. G. Song, Z. B. Li and T. B. Cao, *Nanoscale*, 2011, **3**, 2703–2708.
77 N. Liu and Y. Gao, *Small*, 2017, **13**, 1701989.
78 N. Kurra, M. K. Hota and H. N. Alshareef, *Nano Energy*, 2015, **13**, 500–508.
79 C. Yin, L. He, Y. Wang, Z. Liu, G. Zhang, K. Zhao, C. Tang, M. Yan, Y. Han and L. Mai, *RSC Adv.*, 2016, **6**, 43436–43441.
80 J. H. Lim, Y. H. Ko, J. W. Leem and J. S. Yu, *Opt. Express*, 2015, **23**, A169–A179.
81 L. Zhang, C. Su, L. Cheng, N. Y. Cui, L. Gu, Y. Qin, R. S. Yang and F. Zhou, *ACS Appl. Mater. Interfaces*, 2019, **11**, 26824–26829.
82 T. Li, L. Chen, X. Yang, X. Chen, Z. Zhang, T. Zhao, X. Li and J. Zhang, *J. Mater. Chem. C*, 2019, **7**, 1022–1027.
83 S. L. Zhai, W. C. Jiang, L. Wei, H. E. Karahan, Y. Yuan, A. K. Ng and Y. Chen, *Mater. Horiz.*, 2015, **2**, 598–605.
84 K. Dong, Y. C. Wang, J. N. Deng, Y. J. Dai, S. L. Zhang, H. Y. Zou, B. H. Gu, B. Z. Sun and Z. L. Wang, *ACS Nano*, 2017, **11**, 9490–9499.
85 T. J. Mun, S. H. Kim, J. W. Park, J. H. Moon, Y. Jang, C. Huynh, R. H. Baughman and S. J. Kim, *Adv. Funct. Mater.*, 2020, **30**, 2000411.
86 X. Y. Liu, X. X. Jin, L. Li, J. F. Wang, Y. Y. Yang, Y. X. Cao and W. J. Wang, *J. Mater. Chem. A*, 2020, **8**, 12526–12537.
87 S. Kwon, T. Lee, H. J. Choi, J. Ahn, H. Lim, G. Kim, K. B. Choi and J. J. Lee, *J. Power Sources*, 2021, **481**, 228939.
88 X. Wang, S. Zheng, F. Zhou, J. Qin, X. Shi, S. Wang, C. Sun, X. Bao and Z. S. Wu, *Natl. Sci. Rev.*, 2019, **7**, 64–72.
89 R. Cao, J. Wang, S. Zhao, W. Yang, Z. Yuan, Y. Yin, X. Du, N. W. Li, X. Zhang and X. Li, *Nano Res.*, 2017, **11**, 3771–3779.
90 X. W. Xu, M. Luo, P. He, X. J. Guo and J. L. Yang, *Appl. Phys. A: Solids Surf.*, 2019, **125**, 714.
91 S. Zheng, H. Wang, P. Das, Y. Zhang, Y. Cao, J. Ma, S. F. Liu and Z. Wu, *Adv. Mater.*, 2021, **33**, 202005449.
92 H. Shahariar, I. Kim, H. Soewardiman and J. S. Jur, *ACS Appl. Mater. Interfaces*, 2019, **11**, 6208–6216.
93 T. Cheng, Y. Wu, Y. Chen, Y. Zhang, W. Lai and W. Huang, *Small*, 2019, **15**, 1901830.
94 H. Guo, Z. Jiang, D. Y. Ren, S. X. Li, J. L. Wang, X. B. Cai, D. X. Zhang, Q. Q. Guo, J. F. Xiao and J. Yang, *Chemelectrochem*, 2021, **8**, 1574–1579.
95 T. Cheng, Y. Z. Zhang, J. P. Yi, L. Yang, J. D. Zhang, W. Y. Lai and W. Huang, *J. Mater. Chem. A*, 2016, **4**, 13754–13763.
96 D. Cao, Y. Xing, K. Tantratian, X. Wang, Y. Ma, A. Mukhopadhyay, Z. Cheng, Q. Zhang, Y. Jiao and L. Chen, *Adv. Mater.*, 2019, **31**, 1807313.
97 T. Kim, S. Jeon, S. Lone, S. J. Doh, D.-M. Shin, H. K. Kim, Y.-H. Hwang and S. W. Hong, *Nano Energy*, 2018, **54**, 209–217.
98 M. Liu, X. Pu, Z. Cong, Z. Liu, T. Liu, Y. Chen, J. Fu, W. Hu and Z. L. Wang, *ACS Appl. Mater. Interfaces*, 2019, **11**, 5095–5106.
99 X. C. Tian, J. Jin, S. Q. Yuan, C. K. Chua, S. B. Tor and K. Zhou, *Adv. Energy Mater.*, 2017, **7**, 1700127.
100 K. Chatterjee and T. K. Ghosh, *Adv. Mater.*, 2020, **32**, 1902086.
101 P. J. Kelly and R. D. Arnell, *Vacuum*, 2000, **56**, 159–172.
102 W. K. Sang, H. Y. Jin, B. Son, Y. G. Lee, K. M. Kim, M. L. Yong and K. Y. Cho, *Adv. Mater.*, 2014, **26**, 2977–2982.
103 L. He, T. Hong, X. Hong, X. Liao, Y. Chen, W. Zhang, H. Liu, W. Luo and L. Mai, *Energy Technol.*, 2019, **7**, 1900144.
104 D. C. Lin, Y. Y. Liu and Y. Cui, *Nat. Nanotechnol.*, 2017, **12**, 194–206.
105 W. M. Kang, N. P. Deng, J. G. Ju, Q. X. Li, D. Y. Wu, X. M. Ma, L. Li, M. Naebe and B. W. Cheng, *Nanoscale*, 2016, **8**, 16541–16588.
106 M. S. Whittingham, *Chem. Rev.*, 2004, **104**, 4271–4301.
107 Z. Y. Wang, Q. X. Li, S. Qin, D. Liu, P. Zhang, D. Hegh, J. Z. Zhang, M. Naebe, W. W. Lei and J. M. Razal, *J. Power Sources*, 2021, **489**, 229464.
108 J. Duan, Y. H. Zheng, W. Luo, W. Y. Wu, T. R. Wang, Y. Xie, S. Li, J. Li and Y. H. Huang, *Natl. Sci. Rev.*, 2020, **7**, 1208–1217.
109 K. Yan, Z. D. Lu, H. W. Lee, F. Xiong, P. C. Hsu, Y. Z. Li, J. Zhao, S. Chu and Y. Cui, *Nat. Energy*, 2016, **1**, 16010.
110 L. He, H. Liu, W. Luo, W. Zhang, X. Liao, Y. Guo, T. Hong, H. Yuan and L. Mai, *Appl. Phys. Lett.*, 2019, **114**, 223903.

111 S. Yoneoka, J. Lee, M. Liger, G. Yama, T. Kodama, M. Gunji, J. Provine, R. T. Howe, K. E. Goodson and T. W. Kennyt, *Nano Lett.*, 2012, **12**, 683–686.
112 Y. H. Lin, Y. C. Hsueh, P. S. Lee, C. C. Wang, J. M. Wu, T. P. Perng and H. C. Shih, *J. Mater. Chem.*, 2011, **21**, 10552–10558.
113 M. Knez, K. Niesch and L. Niinisto, *Adv. Mater.*, 2007, **19**, 3425–3438.
114 A. M. Schwartzberg and D. Olynick, *Adv. Mater.*, 2015, **27**, 5778–5784.
115 J. Lee, J. Yoon, H. G. Kim, S. Kang, W. S. Oh, H. Algadi, S. Al-Sayari, B. Shong, S. H. Kim, H. Kim, T. Lee and H. B. R. Lee, *NPG Asia Mater.*, 2016, **8**, e331.
116 G. Marin, R. Funahashi and M. Karppinen, *Adv. Eng. Mater.*, 2020, **22**, 2000535.
117 Z. H. Guo, M. M. Liu, Z. F. Cong, W. B. Guo, P. P. Zhang, W. G. Hu and X. Pu, *Adv. Mater. Technol.*, 2020, **5**, 2000544.
118 F. J. Miao, C. L. Shao, X. H. Li, K. X. Wang and Y. C. Liu, *J. Mater. Chem. A*, 2016, **4**, 4180–4187.
119 L. Chen, L. N. Chen, Q. Ai, D. P. Li, P. C. Si, J. K. Feng, L. Zhang, Y. H. Li, J. Lou and L. J. Ci, *Chem. Eng. J.*, 2018, **334**, 184–190.
120 S. Seyedin, S. Uzun, A. Levitt, B. Anasori, G. Dion, Y. Gogotsi and J. M. Razal, *Adv. Funct. Mater.*, 2020, **30**, 1910504.
121 Y. Huang, W. S. Ip, Y. Y. Lau, J. F. Sun, J. Zeng, N. S. S. Yeung, W. S. Ng, H. F. Li, Z. X. Pei, Q. Xue, Y. K. Wang, J. Yu, H. Hu and C. Y. Zhi, *ACS Nano*, 2017, **11**, 8953–8961.
122 M. F. Lin, J. Q. Xiong, J. X. Wang, K. Parida and P. S. Lee, *Nano Energy*, 2018, **44**, 248–255.
123 J. Wang, S. Huang, X. Lu, Z. Xu, Y. Zhao, J. Li and X. Wang, *J. Mater. Chem. C*, 2017, **5**, 9673–9679.
124 W. Eom, H. Shin, R. B. Ambade, S. H. Lee, K. H. Lee, D. J. Kang and T. H. Han, *Nat. Commun.*, 2020, **11**, 2825.
125 D. Chang, J. Liu, B. Fang, Z. Xu, Z. Li, Y. Liu, L. Brassart, F. Guo, W. Gao and C. Gao, *Science*, 2021, **372**, 614–617.
126 T. Zheng, N. Xu, Q. Kan, H. B. Li, C. R. Lu, P. Zhang, X. D. Li, D. X. Zhang and X. D. Wang, *Polymers*, 2019, **11**, 867.
127 S. Y. Cai, T. Q. Huang, H. Chen, M. Salman, K. Gopalsamy and C. Gao, *J. Mater. Chem. A*, 2017, **5**, 22489–22494.
128 W. Yan, A. Page, N. D. Tung, Y. P. Qu, F. Sordo, L. Wei and F. Sorin, *Adv. Mater.*, 2019, **31**, 1802348.
129 M. Bayindir, F. Sorin, A. F. Abouraddy, J. Viens, S. D. Hart, J. D. Joannopoulos and Y. Fink, *Nature*, 2004, **431**, 826–829.
130 L. Ren, Q. Jiang, K. Y. Chen, Z. P. Chen, C. F. Pan and L. L. Jiang, *Sensors*, 2016, **16**, 908.
131 W. Zeng, X. M. Tao, S. Chen, S. M. Shang, H. L. W. Chan and S. H. Choy, *Energy Environ. Sci.*, 2013, **6**, 2631–2638.
132 X. Shi, Y. Zuo, P. Zhai, J. Shen, Y. Yang, Z. Gao, M. Liao, J. Wu, J. Wang and X. Xu, *Nature*, 2021, **591**, 240–245.
133 Q. Huang, D. Wang and Z. Zheng, *Adv. Energy Mater.*, 2016, **6**, 1600783.
134 Z. Liu, F. Mo, H. Li, M. Zhu, Z. Wang, G. Liang and C. Zhi, *Small Methods*, 2018, **2**, 1800124.
135 C. F. Wang, T. He, J. L. Cheng, Q. Guan and B. Wang, *Adv. Funct. Mater.*, 2020, **30**, 2004430.
136 S. H. Ha, K. H. Shin, H. W. Park and Y. J. Lee, *Small*, 2018, **14**, 1703418.
137 X. Pu, M. Liu, L. Li, S. Han, X. Li, C. Jiang, C. Du, J. Luo, W. Hu and Z. L. Wang, *Adv. Energy Mater.*, 2016, **6**, 1601254.
138 X. M. Lyu, F. H. Su and M. H. Miao, *J. Power Sources*, 2016, **307**, 489–495.
139 A. Levitt, J. Zhang, G. Dion, Y. Gogotsi and J. M. Razal, *Adv. Funct. Mater.*, 2020, **30**, 2000739.
140 S. L. Zhai, H. E. Karahan, L. Wei, Q. H. Qian, A. T. Harris, A. I. Minett, S. Ramakrishna, A. K. Ng and Y. Chen, *Energy Storage Mater.*, 2016, **3**, 123–139.
141 Y. Wang, X. Wang, X. Li, X. Li, Y. Liu, Y. Bai, H. Xiao and G. Yuan, *Adv. Funct. Mater.*, 2020, **31**, 2008185.
142 L. C. Wang, C. G. Zhang, X. Jiao and Z. H. Yuan, *Nano Res.*, 2019, **12**, 1129–1137.
143 I. Nuramdhani, M. Jose, P. Samyn, P. Adriaensens, B. Malengier, W. Deferme, G. De Mey and L. Van Langenhove, *Polymers*, 2019, **11**, 345.
144 S. Kwon, T. Lee, H.-J. Choi, J. Ahn, H. Lim, G. Kim, K.-B. Choi and J. Lee, *J. Power Sources*, 2021, **481**, 228939.
145 X. Guan, J. Gong and B. Xu, *ACS Appl. Mater. Interfaces*, 2020, **12**, 17967–17978.
146 Q. Y. Huang, D. R. Wang, H. Hu, J. Shang, J. Chang, C. Xie, Y. Yang, X. Lepro, R. H. Baughman and Z. J. Zheng, *Adv. Funct. Mater.*, 2020, **30**, 1910541.
147 Z. S. Chai, N. N. Zhang, P. Sun, Y. Huang, C. X. Zhao, H. J. Fang, X. Fan and W. J. Mai, *ACS Nano*, 2016, **10**, 9201–9207.
148 J. Lin, Z. W. Peng, Y. Y. Liu, F. Ruiz-Zepeda, R. Q. Ye, E. L. G. Samuel, M. J. Yacaman, B. I. Yakobson and J. M. Tour, *Nat. Commun.*, 2014, **5**, 5714.
149 L. Thekkekara and M. Gu, *Sci. Rep.*, 2019, **9**, 11822.
150 J. Chen, Y. Huang, N. N. Zhang, H. Y. Zou, R. Y. Liu, C. Y. Tao, X. Fan and Z. L. Wang, *Nat. Energy*, 2016, **1**, 16138.
151 M. Tanrioven, *J. Power Sources*, 2005, **150**, 136–149.
152 C. Xu and Z. L. Wang, *Adv. Mater.*, 2011, **23**, 873–877.
153 R. Wu, L. Ma, C. Hou, Z. Meng, W. Guo, W. Yu, R. Yu, F. Hu and X. Y. Liu, *Small*, 2019, **15**, 1901558.
154 Y. Tan, K. Ivanov, Z. Mei, H. Li, H. Li, L. Lubich, C. Wang and L. Wang, *Micromachines*, 2021, **12**, 110.
155 D. Teichmann, A. Kuhn, S. Leonhardt and M. Walter, *Sensors*, 2014, **14**, 1039–1056.
156 S. Seyedin, P. Zhang, M. Naebe, S. Qin, J. Chen, X. Wang and J. M. Razal, *Mater. Horiz.*, 2019, **6**, 219–249.
157 M. Ha, S. Lim and H. Ko, *J. Mater. Chem. B*, 2018, **6**, 4043–4064.
158 C. L. Choong, M. B. Shim, B. S. Lee, S. Jeon, D. S. Ko, T. H. Kang, J. Bae, S. H. Lee, K. E. Byun, J. Im, Y. J. Jeong, C. E. Park, J. J. Park and U. I. Chung, *Adv. Mater.*, 2014, **26**, 3451–3458.
159 F. Pizarro, P. Villavicencio, D. Yunge, M. Rodriguez, G. Hermosilla and A. Leiva, *Sensors*, 2018, **18**, 1190.
160 G. Zhu, W. Q. Yang, T. J. Zhang, Q. S. Jing, J. Chen, Y. S. Zhou, P. Bai and Z. L. Wang, *Nano Lett.*, 2014, **14**, 3208–3213.

161 Y. Huang, M. Zhong, Y. Huang, M. S. Zhu, Z. X. Pei, Z. F. Wang, Q. Xue, X. M. Xie and C. Y. Zhi, *Nat. Commun.*, 2015, **6**, 10310.
162 L. Chen, M. Lu, H. Yang, J. R. Salas Avila, B. Shi, L. Ren, G. Wei, X. Liu and W. Yin, *ACS Nano*, 2020, **14**, 8191–8201.
163 J. Lee, H. Kwon, J. Seo, S. Shin, J. H. Koo, C. Pang, S. Son, J. H. Kim, Y. H. Jang and D. E. Kim, *Adv. Mater.*, 2015, **27**, 2433–2439.
164 C. C. Vu and J. Kim, *Sens. Actuators, A*, 2020, **314**, 112029.
165 K. Keum, J. S. Heo, J. Eom, K. W. Lee, S. K. Park and Y.-H. Kim, *Sensors*, 2021, **21**, 442.
166 K. I. Park, J. H. Son, G. T. Hwang, C. K. Jeong, J. Ryu, M. Koo, I. Choi, S. H. Lee, M. Byun and Z. L. Wang, *Adv. Mater.*, 2014, **26**, 2514–2520.
167 Y. Su, C. Chen, H. Pan, Y. Yang, G. Chen, X. Zhao, W. Li, Q. Gong, G. Xie and Y. Zhou, *Adv. Funct. Mater.*, 2021, **31**, 2010962.
168 D. Matsouka, S. Vassiliadis and D. V. Bayramol, *Mater. Res. Express*, 2018, **5**, 065508.
169 M. Ha, J. Park, Y. Lee and H. Ko, *ACS Nano*, 2015, **9**, 3421–3427.
170 X. Tong, Z. Tian, J. Sun, V. Tung, R. B. Kaner and Y. Shao, *Mater. Today*, 2021, **44**, 78–104.
171 D. Chen, D. Wang, Y. Yang, Q. Huang, S. Zhu and Z. Zheng, *Adv. Energy Mater.*, 2017, **7**, 1700890.
172 B. J. Blaiszik, S. L. B. Kramer, S. C. Olugebefola, J. S. Moore, N. R. Sottos and S. R. White, *Annu. Rev. Mater. Res.*, 2010, **40**, 179–211.
173 S. R. White, N. R. Sottos, P. H. Geubelle, J. S. Moore, M. R. Kessler, S. R. Sriram, E. N. Brown and S. Viswanathan, *Nature*, 2001, **409**, 794–797.
174 K. S. Toohey, N. R. Sottos, J. A. Lewis, J. S. Moore and S. R. White, *Nat. Mater.*, 2007, **6**, 581–585.
175 E. B. Murphy, E. Bolanos, C. Schaffner-Hamann, F. Wudl, S. R. Nutt and M. L. Auad, *Macromolecules*, 2008, **41**, 5203–5209.
176 G. Ge, Y.-Z. Zhang, W. Zhang, W. Yuan, J. K. El-Demellawi, P. Zhang, E. Di Fabrizio, X. Dong and H. N. Alshareef, *ACS Nano*, 2021, **15**, 2698–2706.
177 H. L. Qin, T. Zhang, N. Li, H. P. Cong and S. H. Yu, *Nat. Commun.*, 2019, **10**, 2202.
178 Z. Zheng, X. Huang, M. Schenderlein, D. Borisova, R. Cao, H. Möhwald and D. Shchukin, *Adv. Funct. Mater.*, 2013, **23**, 3307–3314.
179 R. Wool and K. O'connor, *J. Appl. Phys.*, 1981, **52**, 5953–5963.
180 M. Q. Zhang and M. Z. Rong, *J. Polym. Sci., Part B: Polym. Phys.*, 2012, **50**, 229–241.
181 Y. Cao, T. G. Morrissey, E. Acome, S. I. Allec, B. M. Wong, C. Keplinger and C. Wang, *Adv. Mater.*, 2017, **29**, 1605099.